

**GSFC JPSS CMO
June 3, 2014
Released**

**Joint Polar Satellite System (JPSS) Ground Project
Code 474
474-00034**

**Joint Polar Satellite System (JPSS)
VIIRS Surface Reflectance Algorithm
Theoretical Basis Document (ATBD)**

For Public Release

The information provided herein does not contain technical data as defined in the International Traffic in Arms Regulations (ITAR) 22 CFC 120.10. This document has been approved For Public Release.



National Aeronautics and
Space Administration

**Goddard Space Flight Center
Greenbelt, Maryland**

Joint Polar Satellite System (JPSS) VIIRS Surface Reflectance Algorithm Theoretical Basis Document (ATBD)

JPSS Electronic Signature Page

Prepared By:

Leslie Belsma
JPSS Data Products and Algorithms
(Electronic Approvals available online at https://jpssmis.gsfc.nasa.gov/mainmenu_dsp.cfm)

Approved By:

Eric Gottshall
DPA Manager
(Electronic Approvals available online at https://jpssmis.gsfc.nasa.gov/mainmenu_dsp.cfm)

Goddard Space Flight Center
Greenbelt, Maryland

Preface

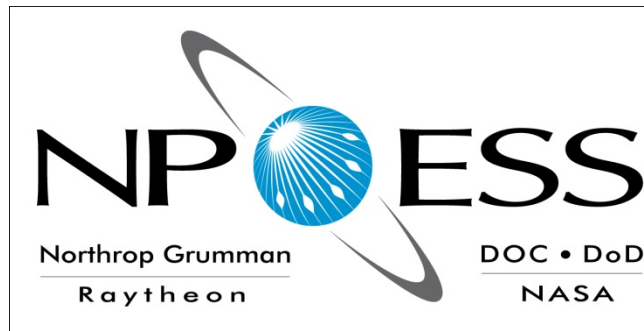
This document is under JPSS Ground AERB configuration control. Once this document is approved, JPSS approved changes are handled in accordance with Class I and Class II change control requirements as described in the JPSS Configuration Management Procedures, and changes to this document shall be made by complete revision.

Any questions should be addressed to:

JPSS Ground Project Configuration Management Office
NASA/GSFC
Code 474
Greenbelt, MD 20771

Change History Log

Revision	Effective Date	Description of Changes (Reference the CCR & CCB/ERB Approve Date)
Original	04/22/2011	This version incorporates 474-CCR-11-0049 which converts Operational Algorithm Description Document For VIIRS Surface Reflectance Algorithm Basis Document ATBD, Rev A of D43765 to a JPSS document, Rev -. This was approved by the JPSS Ground Algorithm ERB on April 22, 2011.
A	09/18/2013	474-CCR-13-1078: Approved by the JPSS Ground Algorithm ERB on September 18, 2013. Changed Section 2.3 and corrected document title <u>FROM:</u> JPSS Operational Algorithm Description Document For VIIRS Surface Reflectance Algorithm Theoretical Basis Document (ATBD) <u>TO:</u> JPSS VIIRS Surface Reflectance Algorithm Theoretical Basis Document (ATBD).



NATIONAL POLAR-ORBITING OPERATIONAL ENVIRONMENTAL SATELLITE SYSTEM (NPOESS)

OPERATIONAL ALGORITHM DESCRIPTION DOCUMENT FOR VIIRS SURFACE REFLECTANCE ALGORITHM THEORETICAL BASIS DOCUMENT ATBD (REF Y2411) (D43765 Rev A)

CDRL No. A032

Northrop Grumman Space & Mission Systems Corporation
One Space Park
Redondo Beach, California 90278

Copyright © 2004-2009
Northrop Grumman Corporation and Raytheon Company
Unpublished Work
ALL RIGHTS RESERVED

Portions of this work are the copyrighted work of Northrop Grumman and Raytheon. However, other entities may own copyrights in this work.

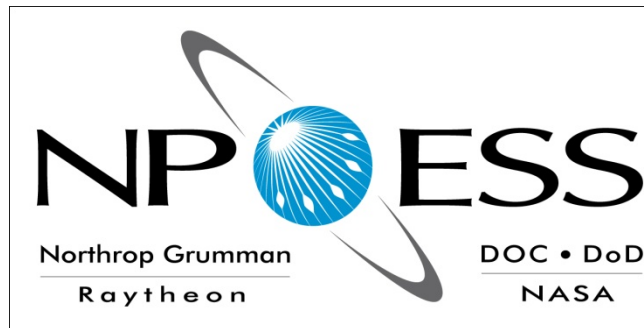
This documentation/technical data was developed pursuant to Contract Number F04701-02-C-0502 with the US Government. The US Government's rights in and to this copyrighted data are as specified in DFAR 252.227-7013, which was made part of the above contract.

This document has been identified per the NPOESS Common Data Format Control Book – External Volume 5 Metadata, D34862-05, Appendix B as a document to be provided to the NOAA Comprehensive Large Array-data Stewardship System (CLASS) via the delivery of NPOESS Document Release Packages to CLASS.

The information provided herein does not contain technical data as defined in the International Traffic in Arms Regulations (ITAR) 22 CFR 120.10.

This document has been approved by the United States Government for public release in accordance with NOAA NPOESS Integrated Program Office.

Distribution: Statement A: Approved for public release; distribution is unlimited.



NATIONAL POLAR-ORBITING OPERATIONAL ENVIRONMENTAL SATELLITE SYSTEM (NPOESS)

OPERATIONAL ALGORITHM DESCRIPTION DOCUMENT FOR VIIRS SURFACE REFLECTANCE ALGORITHM THEORETICAL BASIS DOCUMENT ATBD (REF Y2411) (D43765 Rev A)

PREPARED BY:

Dr Alain Sei, AM&S FV IP Lead
Paul D. Siebels, IDPS PRO SW Manager

ELECTRONIC APPROVAL SIGNATURES:

Roy Tsugawa _____ Date
Algorithm & Data Processing IPT Lead &
Algorithm Change Control Board Chairperson

Gerald J. Mulvey _____ Date
Senior Systems Engineer


			
Revision/Change Record			Document Number D43765
Revision	Document Date	Revision/Change Description	Pages Affected
---	1/26/2007	Initial PCIM Release to bring document into Matrix Accountability. Reference original document number: Y2411 delivered in 2004	All
A	12/09/08	Corrections due to RFA for CDA reviewed as Raytheon R5v8 ECR A205. Approved for Public Release per Contracts letter 090618-01.	iv-xi, 1, 5, 7, 9-12, 15, 17-20, 22-31, 33-40

TABLE OF CONTENTS

	<u>Page</u>
GLOSSARY OF ACRONYMS.....	xi
ABSTRACT	xiv
1.0 INTRODUCTION.....	1
1.1 PURPOSE	1
1.2 SCOPE	1
1.3 VIIRS DOCUMENTS.....	1
1.4 REVISION HISTORY	3
2.1 OBJECTIVES OF SURFACE REFLECTANCE RETRIEVALS.....	5
2.2 INSTRUMENT CHARACTERISTICS.....	6
2.3 RETRIEVAL STRATEGY	11
3.0 ALGORITHM DESCRIPTION.....	13
3.1 PROCESSING OUTLINE	13
3.2 ALGORITHM INPUT	15
3.2.1 VIIRS Data	15
3.2.2 Non-VIIRS Data.....	15
3.3 ALGORITHM OUTPUT.....	16
3.4 THEORETICAL DESCRIPTION—PHYSICS AND MATHEMATICAL	
BACKGROUND	16
3.4.1. Introduction.....	16
3.4.2 Lambertian correction	17
3.4.2.1 Formalism.....	17
3.4.2.2 Lambertian infinite target correction implementation	18
3.4.2.3 Lambertian infinite target correction operational approach.....	19
3.4.3 Adjacency Adjustment.....	22
3.4.3.1 Formalism.....	22
3.4.3.2 Correction for adjacency effect-implementation	24
3.4.3.3 Correction for adjacency effect-operational approach	25
3.4.4 BRDF atmosphere coupling correction	25
3.4.4.1 Formalism.....	25
3.4.4.2 BRDF atmosphere coupling correction Implementation	26
3.4.4.3 BRDF atmosphere coupling correction-operational approach	27
3.4.5 Thin Cirrus Correction.....	29
3.5 ALGORITHM VERIFICATION.....	30
3.5.1 Preliminary Verification Test.....	31
3.5.1.1 Test Scenes	31

3.5.1.2	Results	327
3.5.1.3	Summary	33
3.5.2	PREVIOUS SIMULATION TESTS.....	33
3.6	ALGORITHM VALIDATION.....	34
3.6.1	Pre-Launch Algorithm Test/Development Activities.....	34
3.6.2	Post-Launch Algorithm Test/Development Activities	35
3.7	PRACTICAL CONSIDERATIONS	37
3.7.1	Numerical Computation Considerations	37
3.7.2	Programming and Procedural Considerations.....	37
3.7.3	Configuration of Retrievals	38
3.7.4	Quality Assessment and Diagnostics	39
3.7.5	Exception Handling.....	39
4.0	ASSUMPTIONS AND LIMITATIONS	40
4.1	ASSUMPTIONS.....	40
4.2	LIMITATIONS.....	40
5.0	REFERENCES	41

LIST OF FIGURES

	<u>Page</u>
Figure 1. Summary of VIIRS design concepts and heritage.....	7
Figure 2. VIIRS detector footprint aggregation scheme for building "pixels." Dimensions are approximate; please see the VIIRS Sensor Specification for the current values.	8
Figure 3. Benefits of VIIRS aggregation scheme in reducing pixel growth at edge of scan. Switch-point angles are approximate and may be out of date; please see the VIIRS Sensor Specification for the current values.	8
Figure 4. VIIRS spectral bands, visible and near infrared.	10
Figure 5. VIIRS spectral bands, short wave infrared.	10
Figure 6. Surface Reflectance IP processing architecture.	14
Figure 7. The atmospheric components affecting the remote sensing signal in the 0.4-2.5 μm range...	17
Figure 8: Atmospheric environment function as a function of the distance from the target center, for molecules and aerosols.	23
Figure 9. Relationship between BRDF shape and NDVI.	29
Figure 10. Test scenes centered over (a) the southwestern United States (i.e. 'bright' target area) and (b) the Amazon (i.e. 'dark' target area) used for the VIIRS Surface Reflectance algorithm validation.	32

LIST OF TABLES

Page

Table 1. The twelve VIIRS spectral bands in which Surface Reflectance will be computed.....9

Table 2. Transmittance in the spectral regions corresponding to VIIRS spectral bands at solar and viewing zenith angles equal to 30 degrees and the standard US 62 Atmospheric profile. Adapted from Vermote and Vermeulen (1998).11

Table 3. Retrieved atmospherically corrected Surface Reflectance Values-Arizona Scene.33

Table 4. Retrieved atmospherically corrected Surface Reflectance Values-Amazon Scene.....33

Table 5. Configuration of parameters for Surface Reflectance retrievals.38

Table 6. Exception sources and handling strategies for Surface Reflectance retrievals.....39

GLOSSARY OF ACRONYMS

3D	Three Dimensional
6S	Second Simulation of the Satellite Signal in the Solar Spectrum
AERONET	Aerosol Robotic Network
AOT	Aerosol Optical Thickness
ASAS	Advanced Solid-state Array Spectroradiometer
ATBD	Algorithm Theoretical Basis Document
AVHRR	Advanced Very High Resolution Radiometer
BOREAS	Boreal Ecosystem/Atmosphere Study
BRDF	Bidirectional Reflectance Distribution Function
CMIS	Conical-scanning Microwave Imager/Sounder
DoD	Department of Defense
EDC	EROS Data Center
EDR	Environmental Data Record
EOS	Earth Observing System
EROS	Earth Resources Observation and Science
EVI	Enhanced Vegetation Index
FWHM	Full Width Half Maximum
GIFOV	Ground Instantaneous Field of View
GSD	Ground Sample Distance
GTOS	Global Terrestrial Observing System
HIS	Horizontal Sample Interval
HSR	Horizontal Spatial Resolution
I/O	Input/Output
ICD	Interface Control Document
IFOV	Instantaneous Field of View
IP	Intermediate Product
IPO	Integrated Program Office
LAI	Leaf Area Index
LOWTRAN	Low Resolution Atmospheric Radiance and Transmittance Model
LQF	Land Quality Flag(s)

LTER	Long Term Ecological Research
LUT	Lookup Table
MMNSR	Monthly Mean Non-Snow Reflectance
MODIS	Moderate Resolution Imaging Spectroradiometer
MODTRAN	Moderate Resolution Atmospheric Radiance and Transmittance Model
MTF	Modulation Transfer Function
NASA	National Aeronautics and Space Administration
NCEP	National Centers for Environmental Prediction
NDVI	Normalized Difference Vegetation Index
NOAA	National Oceanic and Atmospheric Administration
NOGAPS	Navy Operational Global Atmospheric Prediction System
NPOESS	National Polar-orbiting Operational Environmental Satellite System
NPP	NPOESS Preparatory Project
OLS	Optical Line Scanner
OMPS	Ozone Mapping Profiling Suite
PARABOLA	Portable Apparatus for Rapid Acquisition of Bidirectional Observations of Land and Atmosphere
POLDER	Polarization and Directionality of the Earth's Reflectances
QC	Quality Control
RMS	Root Mean Square
RSR	Relative Spectral Response
RT	Radiative Transfer
SBRS	Santa Barbara Remote Sensing
SDR	Sensor Data Record
SDSM	Solar Diffuser Stability Monitor
SeaWiFS	Sea-viewing Wide Field-of-view Sensor
SNR	Signal to Noise Ratio
SRD	Sensor Requirements Document
SWIR	Short Wave Infrared
TBD	To Be Determined
TERCAT	Terrain Categorization
THEMIS	Thermal Emission Imaging System

TIROS	Television/Infrared Observation Satellite
TM	Thematic Mapper
TOA	Top of Atmosphere
TOC	Top of Canopy
USGS	United States Geological Survey
VIIRS	Visible/Infrared Imager Radiometer Suite
VNIR	Visible/Near Infrared

ABSTRACT

The algorithm described in this document produces the Surface Reflectance Intermediate Product (IP), one of over thirty products to be generated from the National Polar-orbiting Operational Environmental Satellite System (NPOESS) Visible/Infrared Imager/Radiometer Suite (VIIRS), scheduled for launch late in the first decade of the 21st century. The VIIRS prototype will be carried onboard the NPOESS Preparatory Project (NPP) spacecraft to be launched by the National Aeronautics and Space Administration (NASA). The Surface Reflectance IP consists of directional surface reflectance values in bands centered at 0.412 μm , 0.445 μm , 0.488 μm , 0.555 μm , 0.645 μm , 0.672 μm , 0.865 μm (two different spatial resolutions), 1.24 μm , 1.61 μm (two different spatial resolutions), and 2.25 μm . It is an algorithm for surface reflectance retrieval that has been derived from Moderate Resolution Imaging Spectroradiometer.

The algorithm is designed to contain four modular components, namely, 'Extract inputs', 'Quality Flags', 'Surface Reflectance Retrieval', and 'Write Surface Reflectance IP'. The 'Surface Reflectance Retrieval' component consists of the Lambertian approximation/dynamic atmospheric adjustment, adjacency adjustment, and the bi-directional reflectance distribution function (BRDF) coupling adjustment. The 'Surface Reflectance Retrieval' component corrects for the effects of atmospheric gaseous absorption, molecular and aerosol scattering, thin cirrus contamination, glare from surrounding surface pixels (adjacency effects), and the coupling of the atmosphere and the surface bidirectional reflectance as a function of the viewing and solar geometries, elevation of the target and spectral band assuming a Lambertian surface. The atmospheric adjustment (within the 'Surface Reflectance Retrieval' component) includes 'near-real-time' updates of total column water vapor, ozone, and aerosol optical thickness data input fields. The surface reflectance values are subsequently corrected for adjacency and bi-directional reflectance distribution function (BRDF) effects. The aerosol information comes from the VIIRS Aerosol Optical Thickness IP. The total column water, column ozone, and surface pressure presently come from National Centers for Environmental Prediction (NCEP) feeds. Backup for water vapor comes from the VIIRS Precipitable Water and column ozone from the Ozone Mapping Profiling Suite (OMPS).

This document presents the theoretical basis of the Surface Reflectance IP algorithm. It is not meant to contain detailed information about the code design, the program data language, or code implementation. These details are given in the Operational Algorithm Description document (OAD) for this product.

1.0 INTRODUCTION

Section 1 of the VIIRS Surface Reflectance Intermediate Product (IP) algorithm theoretical basis document (ATBD) describes the purpose and scope of the document. Section 2 provides an overview of the algorithm, and rationale for its configuration. The processing concept and algorithm description are presented in Section 3. Section 4 summarizes assumptions and limitations, and Section 5 contains references for publications cited in the text.

1.1 PURPOSE

This Algorithm Theoretical Basis Document (ATBD) describes the physical and mathematical theory underlying the algorithms used to retrieve the Surface Reflectance Intermediate Product (IP) from Visible/Infrared Imager/Radiometer Suite (VIIRS) Sensor Data Records (SDRs) and ancillary data. It also includes top-level implementation details.

1.2 SCOPE

This document covers the algorithm theoretical basis for the Surface Reflectance IP. Other post-launch products are not discussed. This document is not meant to contain detailed information about the design of the surface reflectance IP code, architecture, program data language, or other relevant items such as land remote sensing gridded data records. It does provide a summary of the processing concept. For a detailed discussion of software implementation, the reader is directed to [Y2469], [Y2474], [Y2483], and [Y2498]. The algorithms for gridding and compositing gridded derived products directly from the Surface Reflectance IP are described in the Earth Gridding ATBD [Y7051]. This document does include a discussion of the uncertainties due to errors in the Surface Reflectance IP algorithm and its multiple input parameters.

1.3 VIIRS DOCUMENTS

References to VIIRS documents will be indicated by Raytheon Santa Barbara Remote Sensing (SBRS) official Y-numbers in italicized brackets, e.g., [Y2388].

Y2387	VIIRS Soil Moisture ATBD
Y2388	VIIRS Aerosol Optical Thickness and Particle Size ATBD
Y2390	VIIRS Suspended Matter ATBD
Y2393	VIIRS Cloud Effective Particle Size and Cloud Optical Thickness ATBD
Y2398	VIIRS Surface Albedo ATBD
Y2400	VIIRS Vegetation Index ATBD
Y2401	VIIRS Snow Cover ATBD

Y2402 VIIRS Surface Type ATBD

Y2404 VIIRS Fresh Water Ice ATBD (product is pending cancellation)

Y2409 VIIRS Sea Ice Age/Edge Motion ATBD

Y2412 VIIRS Cloud Mask ATBD

Y2466 VIIRS Imagery ATBD

Y2468 VIIRS Operations Concept Document

Y2469 VIIRS Context Level Software Architecture

Y2470 VIIRS Interface Control Document

Y2474 VIIRS Land Module Level Software Architecture

Y2483 VIIRS Land Module Level Detailed Design Document

Y2498 VIIRS Surface Reflectance IP Unit Level Detailed Design Document

Y3236 VIIRS Software Integration and Test Plan

Y3237 VIIRS Algorithm Verification and Validation Plan

Y3251 VIIRS Precipitable Water ATBD

Y3252 VIIRS Active Fires ATBD

Y3257 VIIRS Computer Resources Requirements Document

Y3261 VIIRS Radiometric Calibration ATBD

Y3270 VIIRS System Verification and Validation Plan

Y3279 VIIRS Land Module Level Interface Control Document

Y6635 VIIRS Algorithm Software Development Plan

Y6661 VIIRS Algorithm Software Maturity Assessment

Y7040 VIIRS Algorithm/Data Processing Technical Report

Y7051 VIIRS Earth Gridding ATBD

SS154650 VIIRS System Specification

PS154650 VIIRS Sensor Specification

PS154640 VIIRS Algorithm Specification**1.4 REVISION HISTORY**

This is the sixth revision of version 5 of this document. Revision 6 reflects the necessary change to the Lambertian Surface Reflectance algorithm brought on by post-VIIRS Continuation algorithm development work, and includes upgrades to the entire theoretical background section, and a preliminary validation of the algorithm.

The version 5, revision 5 reflects the necessary change from a pure look up table approach described in version 5, revision 4 to a look up table plus equation (hybrid) approach. Revision 5 does not include further development to the thin cirrus adjustment. The specific tasks that have been addressed under revision 5 are:

- Implement the operational MODIS approach consisting of retrieving the surface reflectance after atmospheric corrections without including adjacency and BRDF effects.
- Determine and implement the coefficients used in ozone, oxygen and carbon dioxide corrections for VIIRS bands (as opposed to MODIS bands.)
- Add the MODIS adjacency correction to the algorithm developed.
- Add the MODIS BRDF correction to the algorithm developed.
- Update the system-level sensitivity analyses of the Surface Reflectance IP.

Drs Chengquan Huang, Yunyue (Bob) Yu, and Alain Sei made contributions to Version 5, Revision 5.

Revision 4 contained the following modifications:

- Refinement and simplification of the lookup table (LUT) strategy baselined in Version 4 to separate correction formulae, specifically those for water vapor, column ozone, Rayleigh scattering (surface pressure), and thin cirrus (applied to radiances prior to application of the LUT)
- Establishment of a firmer structure for the Land Quality Flags generated as a part of the Surface Reflectance IP
- Updated VIIRS band characteristics where applicable

Shawn Miller authored version 5, revision 4 of this document, dated May 2002. The changes between version 5, revision 4 and version 5, revision 1 were minor. The only significant modification between version 5, revision 1 and the original version 5 is the addition of a paragraph in section 3.3.2, where a placeholder had been inadvertently retained in the original version 5. The original fifth version of this document was dated March 2002 and was the result of Phase II algorithm development. The document had received modest revisions between Version 4 and Version 5.

The fourth version of this document was dated May 2001. The third version was dated May 2000 at the conclusion of Phase I algorithm development. The second version was dated

June 1999. The first version was dated October 1998. The authors of this document along with authors of previous versions wish to thank Wenge Ni for extensive contributions to earlier versions of this document, and also Alexei Lyapustin and Eric Vermote for numerous insightful discussions of the theoretical basis presented here.

2.0 ALGORITHM OVERVIEW

2.1 OBJECTIVES OF SURFACE REFLECTANCE RETRIEVALS

VIIRS spectral bands contain information about the sensor characteristics, the atmosphere, and primarily from the land surface. The sensor characteristics are generally very well known, while the atmospheric characteristics are not as well known. Further, the atmospheric contribution to the at-satellite signal is much less than the land contribution, especially in most cloud-free conditions. Sensor and atmospheric effects need to be removed to retrieve the surface contribution. This result, usually expressed as a surface reflectance, may then be further refined to yield information useful to land remote sensing applications. The information derived from the surface reflectance and the VIIRS land EDRs could be used to study

- Effects of regional climate variations on agriculture, nutrient fluxes, and ecosystem stress;
- Agricultural and water resources management
- Climate change and weather prediction model outputs, and
- Soil moisture/boundary-layer interfacial parameterizations research, to name a few.

A number of VIIRS products require Surface Reflectance IP values as input. These include: top-of-atmosphere (TOA) and top-of-canopy (TOC) Enhanced Vegetation Index (EVI) and Normalized Difference Vegetation Index (NDVI), which are described in [Y2400]; Surface Type [Y2402]; Surface Albedo [Y2398]; Soil Moisture [Y2387]; Snow Cover [Y2401]; Imagery for sea ice applications [Y2466]; and Sea Ice [Y2409]. Further, the products listed above feed into one another and into other VIIRS products, such as Leaf Area Index (LAI, [Y2400]), and Active Fires [Y3252]. Hence, a need to derive an intermediate product (IP) for VIIRS that contains directional surface reflectance values for all relevant bands, and that accommodates the diverse requirements of the products that use it as input.

The VIIRS surface reflectance algorithm is based on a long heritage most recently coming from MODIS (Vermote et al., 1994; 1997; Vermote and Vermeulen, 1999). The spectral and spatial characteristics of the MODIS sensor are generally similar to the spectral and spatial requirements of the VIIRS sensor.

Operational implementation of the Surface Reflectance IP requires a hybrid approach using radiation transfer (RT) model-derived look-up tables (LUT) and a simple retrieval algorithm. The Second Simulation of the Satellite Signal in the Solar Spectrum (6S) developed at the Laboratoire d'Optique Atmosphérique of Lille, France (Vermote *et al.*, 1997) has been used to generate the LUTs. Other RT models such as MODTRAN 4.0 (Berk *et al.*, 1999) could also be used. The choice to use 6S was based on operational, system specification considerations, and its user friendliness. However, Vermote and Vermeulen (1999) state that the 6S code is only accurate up to the limits of the plane parallel approximation (about 75° zenith angle).

2.2 INSTRUMENT CHARACTERISTICS

The VIIRS instrument is now briefly described to clarify the context of the descriptions of the Surface Reflectance IP presented in this document. VIIRS can be pictured as a convergence of three existing sensors, two of which have seen extensive operational use at this writing. The Operational Linescan System (OLS) is the operational visible/infrared scanner for the Department of Defense (DoD). Its unique strengths are controlled growth in spatial resolution through rotation of the ground instantaneous field of view (GIFOV) and the existence of a low-level light sensor capable of detecting visible radiation at night. OLS has primarily served as a data source for manual analysis of imagery. The Advanced Very High Resolution Radiometer (AVHRR) is the operational visible/infrared sensor flown on the National Oceanic and Atmospheric Administration (NOAA) Television InfraRed Observation Satellite (TIROS-N) series of platforms (Planet, 1988). Its unique strengths are low operational and production cost and the presence of five spectral channels that can be used in a wide number of combinations to produce operational and research products. In December 1999, the National Aeronautics and Space Administration (NASA) launched the Earth Observing System (EOS) morning satellite, *Terra*, which includes the Moderate Resolution Imaging Spectroradiometer (MODIS). This sensor possesses an unprecedented array of thirty-two electro-optical to shortwave infrared spectral bands at resolutions ranging from 250 m to 1 km at nadir, allowing for currently unparalleled accuracy in a wide range of satellite-based environmental measurements.

VIIRS will reside on a platform of the National Polar-orbiting Operational Environmental Satellite System (NPOESS) series of satellites. It is intended to be the product of a convergence between DoD, NOAA and NASA in the form of a single visible/infrared sensor capable of satisfying the needs of all three communities, as well as the research community beyond. As such, VIIRS will require three key attributes: high spatial resolution with controlled growth off nadir; minimal production and operational cost; and a sufficient number of spectral bands to satisfy the requirements for generating accurate operational and scientific products. Figure 1 illustrates the design concept for VIIRS, designed and built by Raytheon Santa Barbara Remote Sensing (SBRS). At its heart is a rotating telescope scanning mechanism that minimizes the effects of solar impingement and scattered light. VIIRS is essentially a combination of Sea-Viewing Wide Field-of-view Sensor (SeaWiFS) fore optics and an all-reflective modification of MODIS/THEMIS aft-optics. Calibration is performed onboard using a solar diffuser for short wavelengths and a blackbody source and deep space view for thermal wavelengths. A solar diffuser stability monitor (SDSM) is also included to track the performance of the solar diffuser. The nominal altitude for NPOESS will be 833 km. The VIIRS scan will therefore extend to 56 degrees on either side of nadir.

The VIIRS Sensor Requirements Document (SRD, IPO [2000]) placed explicit requirements on spatial resolution for the Imagery Environmental Data Record (EDR). Specifically, the horizontal spatial resolution (HSR) of bands used to meet threshold Imagery EDR requirements must be no greater than 400 m at nadir and 800 m at the edge of the scan. This led to the development of a unique scanning approach which optimizes both spatial resolution and signal to noise ratio (SNR) across the scan. The concept is summarized in Figure 2 for the imagery bands; the nested lower resolution radiometric bands follow the same paradigm

at approximately twice the size. The VIIRS detectors are rectangular, with the smaller dimension along the scan. At nadir, three detector footprints are aggregated to form a single VIIRS “pixel.” Moving along the scan away from nadir, the detector footprints become larger both along track and along scan, due to geometric effects and the curvature of the Earth. The effects are much larger along scan. At 31.71 degrees in scan angle, the aggregation scheme is changed from 3x1 to 2x1. A similar switch from 2x1 to 1x1 aggregation occurs at 47.87 degrees. The VIIRS scan consequently exhibits a pixel growth factor of only 2 both along track and along scan, compared with a growth factor of 6 along scan which would be realized without the use of the aggregation scheme. Figure 3 illustrates the benefits of the aggregation scheme for spatial resolution. HSI stands for horizontal sampling interval, the distance between centers of aggregated pixels along-scan. GSD is the ground sample distance between individual detector footprints.

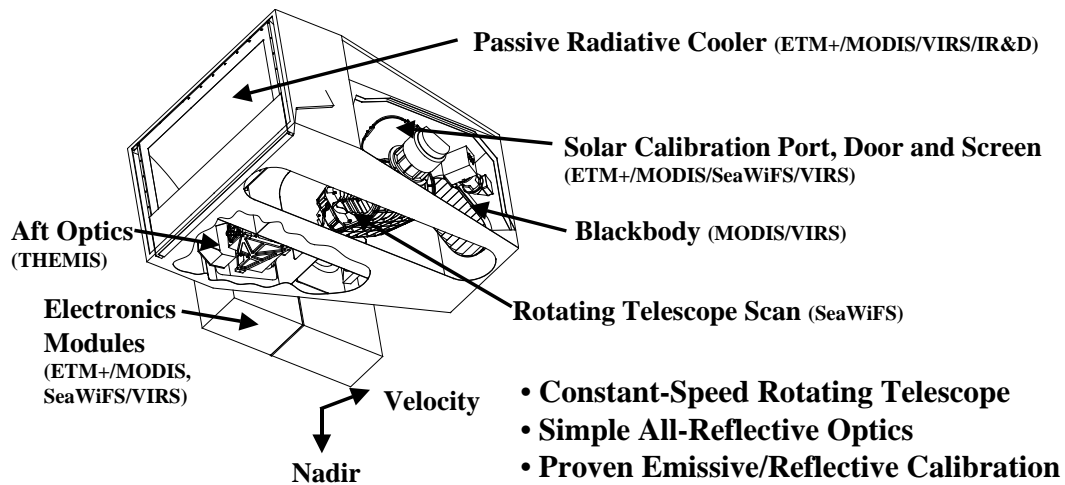


Figure 1. Summary of VIIRS design concepts and heritage.

Fine-Resolution Bands

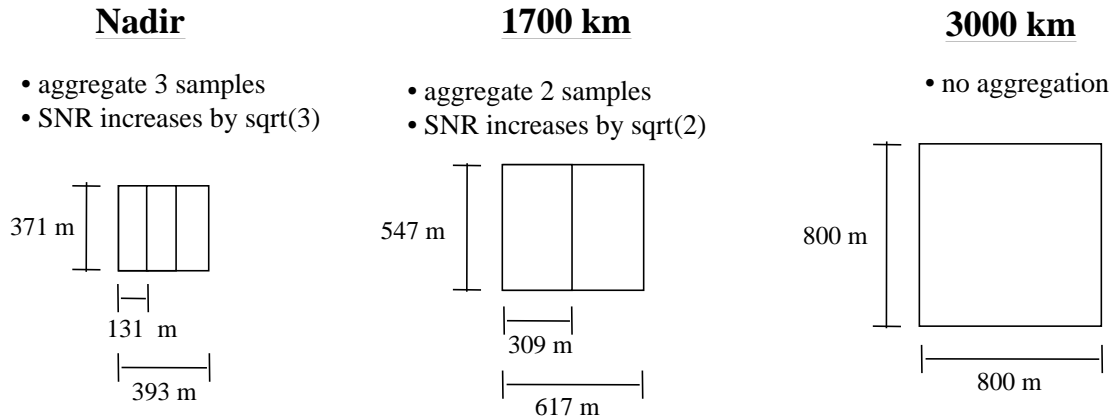


Figure 2. VIIRS detector footprint aggregation scheme for building "pixels." Dimensions are approximate; please see the VIIRS Sensor Specification for the current values.

Scan HSI as a Function of Scan Angle for Unit Raw GSD at Nadir

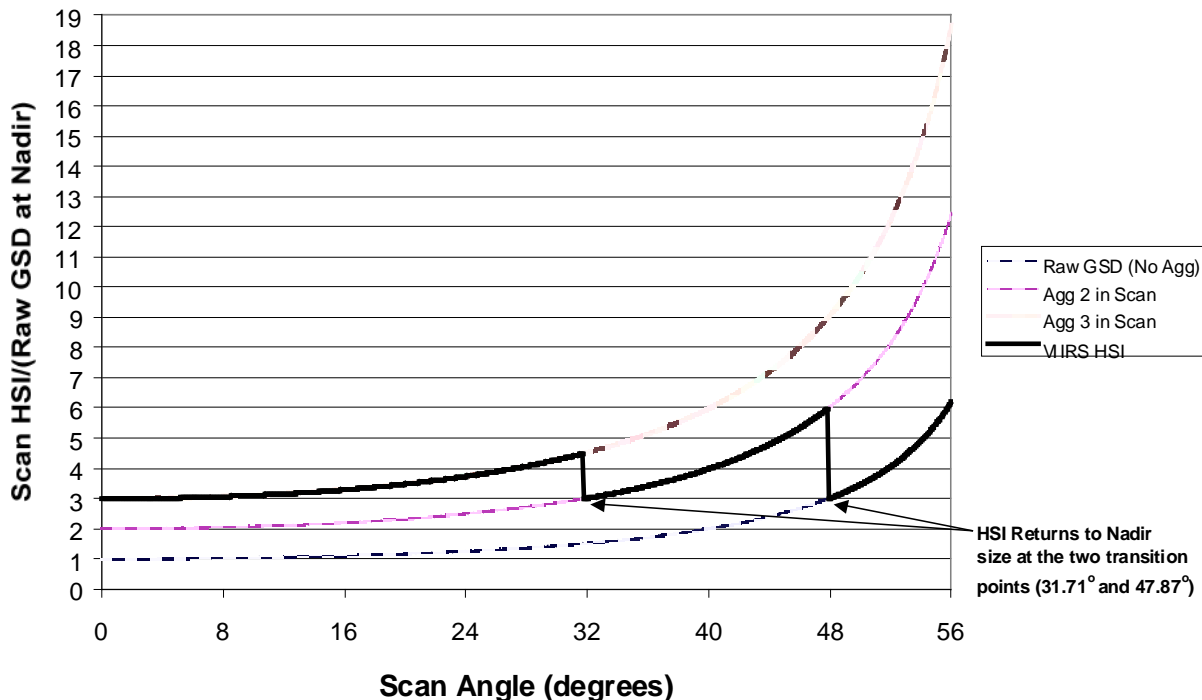


Figure 3. Benefits of VIIRS aggregation scheme in reducing pixel growth at edge of scan. Switch-point angles are approximate and may be out of date; please see the VIIRS Sensor Specification for the current values.

This scanning approach is extremely beneficial for the retrieval of land products such as the NDVI. The increasing importance of land cover change detection makes high spatial resolution in the NDVI and its input reflectances much more important; by comparison, signal to noise ratio (SNR) is a secondary issue (this latter point will be verified later in this document).

The positioning of the VIIRS Visible/Near Infrared (VNIR) and Short Wave Infrared (SWIR) spectral bands is summarized in Figure 4 and Figure 5. The radiometric, spatial, and spectral performances of these bands are summarized in the VIIRS Sensor Specification [PS154650].

The Surface Reflectance IP is delivered for the twelve bands listed in Table 1, and there is a spectral response curve LUT for each band. This strategy minimizes the impact of future spectral response curve algorithm development within the Land Module algorithms. The LUT values reported in this document are based on the relative spectral response (RSR) curves characterized by SBR5 (Y0013276). They are still very similar to the RSR shown in Figure 4 and Figure 5, and hence we chose not to replace these figures in Revision 5.

Table 1. The twelve VIIRS spectral bands in which Surface Reflectance will be computed.

Band Name ^a	Center (microns)	Width ^b (microns)
M1	.415	.020
M2	.445	.020
M3	.490	.020
M4	.555	.020
I1	.640	.075
M5	.673	.021
I2	.865	.039
M7	.865	.039
M8	1.24	.020
I3	1.61	.060
M10	1.61	.060
M11	2.25	.050

^a M indicates band with a nadir resolution of 750 m, I indicates band with a nadir resolution of 375 m. ^b full width half maximum (FWHM)

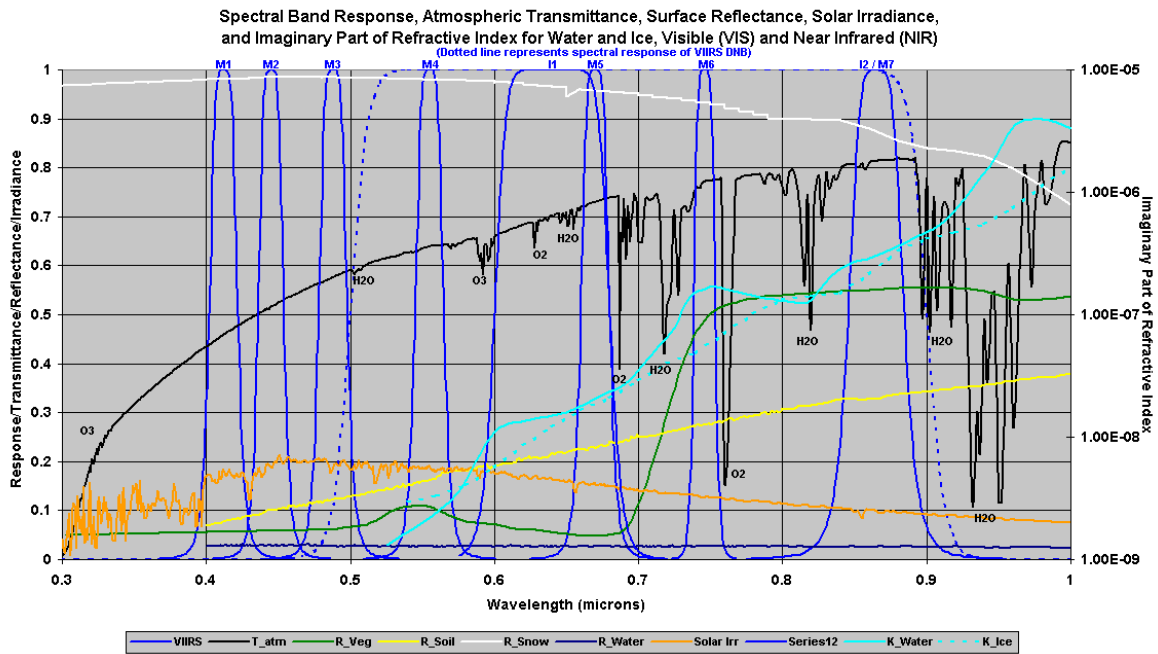


Figure 4. VIIRS spectral bands, visible and near infrared.

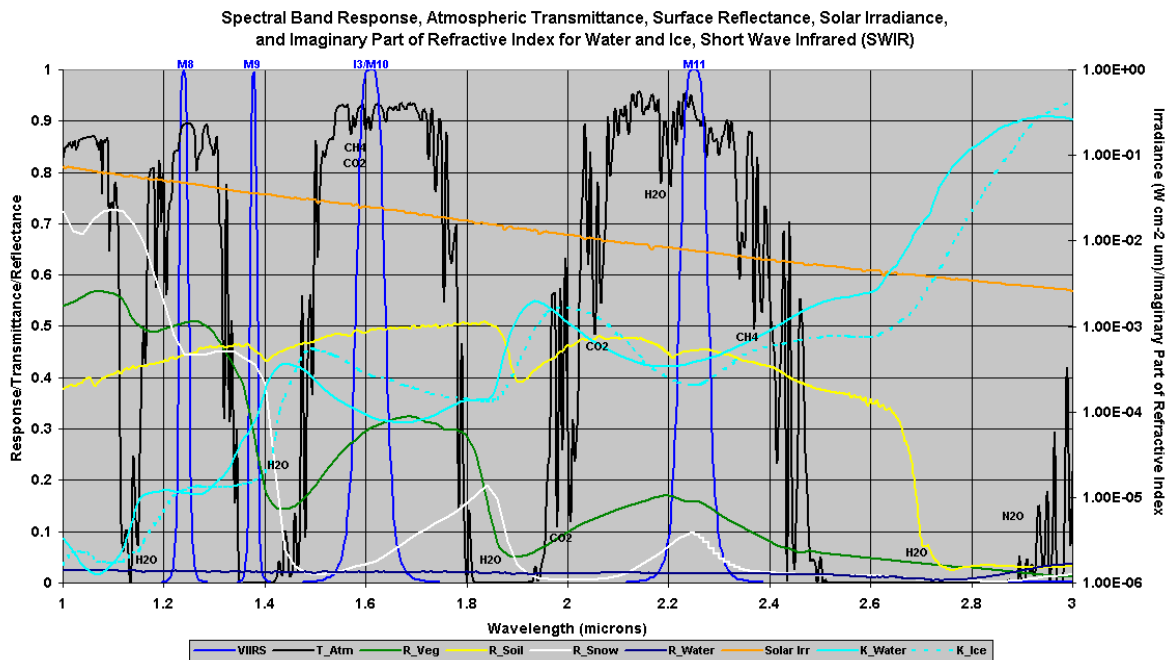


Figure 5. VIIRS spectral bands, short wave infrared.

The VIIRS sensor will be affected by gaseous absorbers, such as water vapor (H_2O), ozone (O_3), carbon dioxide (CO_2), oxygen (O_2), methane (CH_4), nitrous oxide (N_2O), and carbon monoxide (CO). The general attenuation features experienced by the VIIRS sensor are summarized in Table 2.

Table 2. Transmittance in the spectral regions corresponding to VIIRS spectral bands at solar and viewing zenith angles equal to 30 degrees and the standard US 62 Atmospheric profile. Adapted from Vermote and Vermeulen (1998).

VIIRS Band (Table 1)	OZONE		OXYGEN		WATER VAPOR		CARBON DIOXIDE	
	Ave.	Min.	Ave.	Min.	Ave.	Min.	Ave.	Min.
M1	1.0	1.0	1.0	1.0	1.0	1.0	1.0	1.0
M2	0.99	0.99	1.0	1.0	1.0	1.0	1.0	1.0
M3	0.98	0.97	1.0	1.0	1.0	1.0	1.0	1.0
M4	0.94	0.91	1.0	1.0	0.99	0.98	1.0	1.0
I1	0.95	0.92	0.99	0.97	0.98	0.96	1.0	1.0
M5	0.97	0.95	1.0	1.0	0.84	0.67	1.0	1.0
I2	1.0	1.0	1.0	1.0	0.87	0.75	1.0	1.0
M7	1.0	1.0	1.0	1.0	0.87	0.75	1.0	1.0
M8	1.0	1.0	1.0	1.0	1.0	0.99	0.99	0.98
I3	1.0	1.0	1.0	1.0	0.99	0.97	0.95	0.91
M10	1.0	1.0	1.0	1.0	0.99	0.97	0.95	0.91
M11	1.0	1.0	1.0	1.0	0.96	0.93	1.0	1.0

2.3 RETRIEVAL STRATEGY

Retrievals of the Surface Reflectance values will be conducted for all daytime, land pixels within the array of NPOESS/VIIRS swaths. Land pixels are defined by the land/water mask information in the VIIRS Cloud Mask IP. The Surface Reflectance IP is generated in twelve VIIRS spectral bands, listed in Table 1. "Daytime" here is defined by a local solar zenith angle of 85 degrees or less. The limit of 85 degrees on daytime is too high to enable good atmospheric correction, after 75 degrees the solar zenith angle should be flagged as high to reflect the degradation in performance of the atmospheric correction.

Once a pixel has been qualified for retrieval, the Surface Reflectance Unit software is activated using the following baseline inputs: (i) the VIIRS 375-m and 750-m Earth View SDRs [Y3261], which include TOA radiances, solar and viewing geometry, elevation above sea-level (using United States Geologic Survey (USGS), Earth Resources Observing System (EROS) Data Center, GTOPO30 product), (ii) the VIIRS Aerosol Optical Thickness IP [Y2388], (iii) precipitable water from NCEP analyses, (iv) column ozone from NCEP analyses with the Ozone Mapping Profiling Suite (OMPS) as a fallback, (v) surface pressure from NCEP analyses. The elevation above sea level data will be used to refine the spatial resolution the pressure of NCEP. Atmospheric pressure is needed for Rayleigh scattering correction at a spatial resolution of the imagery bands.

The reflectance at the top of the atmosphere is first corrected assuming a lambertian infinite target case. Then an adjacency adjustment is applied to account for contributions from

surrounding pixels. This is followed by a BRDF-coupling adjustment since the land surface is not a lambertian surface. The BRDF-coupling adjustment is based on the RossThick, LiSparse BRDF kernel model. Its three parameters represent the isotropic scattering kernel, volumetric scattering kernel and geometric-optical scattering kernel, respectively. The kernels are developed as functions of solar and viewing geometry. A regression equation featuring NDVI and the Lambertian assumption corrected, adjacency effect adjusted, surface reflectance values are used to derive a weighting parameter set of the three kernels from look up tables (BRDF LUTs). The Surface Albedo IP [Y2398] could be used as a backup source for these kernel values.

3.0 ALGORITHM DESCRIPTION

3.1 PROCESSING OUTLINE

The Surface Reflectance IP algorithm is designed to contain four main subroutines: Extract inputs, Quality Flags, Surface Reflectance Retrieval and Write Surface Reflectance IP. The Surface Reflectance Retrieval subroutine is the main subroutine since it performs the lambertian approximation (atmospheric correction), the adjacency adjustment, and the bidirectional reflectance distribution function (BRDF) coupling adjustment.

The Surface Reflectance Retrieval routine corrects for the effects of gaseous absorption, molecular and aerosol scattering, thin cirrus contamination, glare from surrounding surface pixels (adjacency adjustment), and the coupling of the atmosphere and the surface bidirectional reflectance as a function of the viewing and solar geometries, elevation of the target and spectral band. The atmospheric adjustment (within the 'Surface Reflectance Retrieval' routine) includes updating the correction coefficients with 'in-view' total column water vapor, ozone, and aerosol optical thickness data input fields. The aerosol information required for surface reflectance retrieval comes from the VIIRS Aerosol Optical Thickness (AOT) IP and the Aerosol Model Information IP, complemented by total column water vapor, total column ozone, and surface pressure from National Centers for Environmental Prediction (NCEP) feeds. Backups for these inputs include total column ozone from the Ozone Mapping Profiling Suite (OMPS). The atmospherically corrected surface reflectance values derived using the Lambertian approximation are subsequently adjusted for adjacency and bi-directional reflectance distribution function (BRDF) effects. The BRDF-coupling adjustment is presently designed after the MODIS approach with a slight modification making the isotropic shape parameter a function of the normalized difference vegetation index, NDVI, (Vermote, 2003), an approximation due to operational constraints and the developmental maturity of the MODIS BRDF-coupling adjustment routine. The surface reflectance values after each adjustment are included as data layers in the surface reflectance IP along with the Land Quality Flags. The atmospheric inputs should be available elsewhere, and the solar and viewing geometries are kept as part of the SDR.

Figure 6 shows a snapshot of the architecture for retrieving the Surface Reflectance IP.

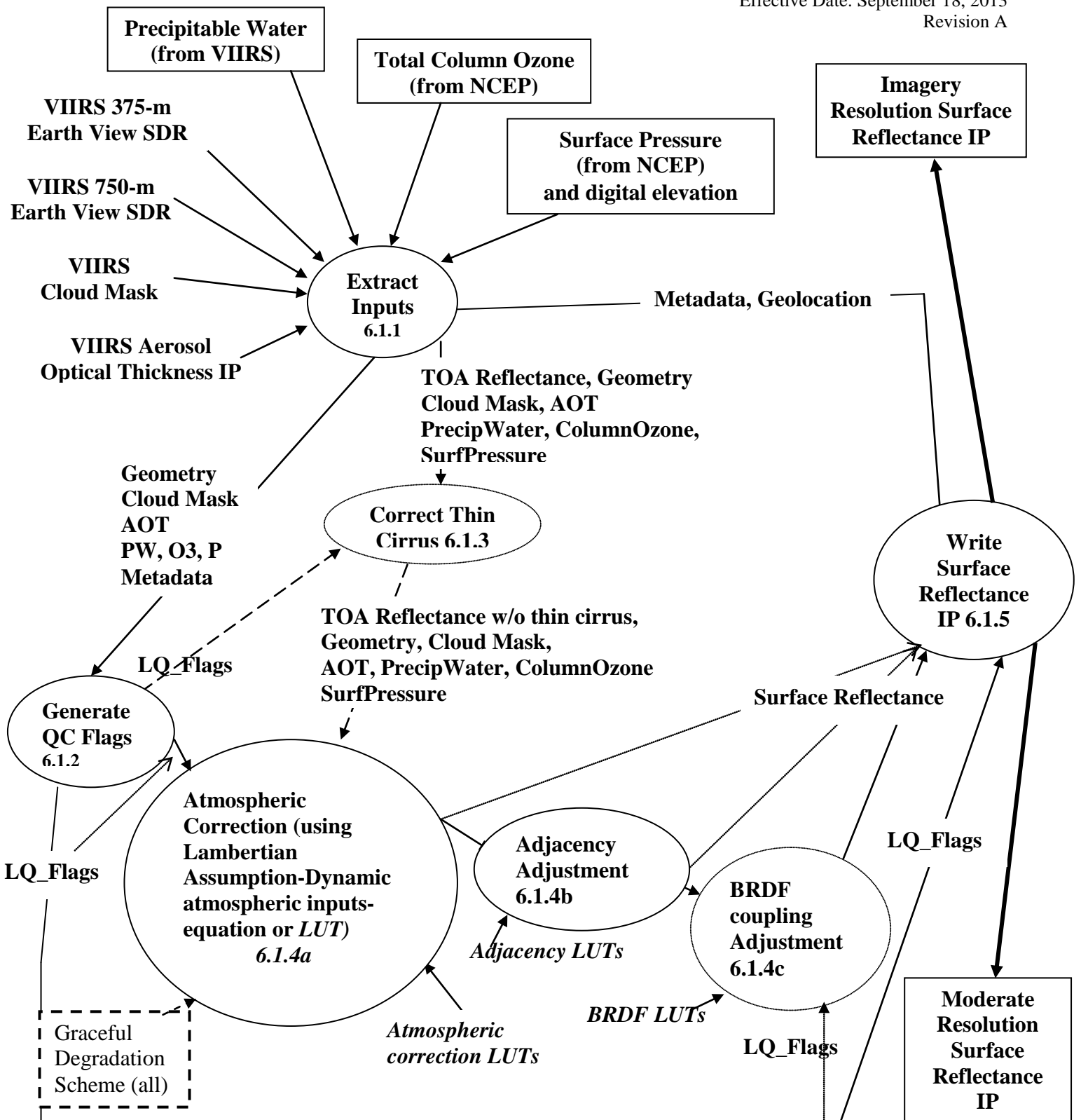


Figure 6. Surface Reflectance IP processing architecture.

The reader is directed to [Y2474] for additional details.

Thin cirrus effects are removed by implementing an empirically based correction using VIIRS band M9 (1.38 μm). The quality control (QC) flags generated from the Build SDR module and the cloud and aerosol quality flag inputs are fused into a single Land Quality Flag (LQF) structure that applies to the Surface Reflectance IP, the Surface Albedo EDR [Y2398], the Vegetation Index EDR [Y2400], the Surface Type EDR [Y2402]. The LQF output is appended to the Surface Reflectance IP. Then the heart of the surface reflectance retrieval process begins, by converting the cirrus effects adjusted satellite reflectance values into surface reflectance values assuming the surface is Lambertian. The earth's surface is generally not Lambertian, and as a result a further correction is applied. The conversion of the at-satellite-reflectance values to surface reflectance requires (i) the use of a set of conversion equations that also account for first order atmospheric multiple scattering effects, and (ii) inputs from pre-generated look up tables (LUTs) and analytic equations for gaseous or molecular effect.

The Lambertian surface reflectance value is passed simultaneously into the adjacency subroutine and to the 'write surface reflectance IP' routine. The output of the adjacency adjustment subroutine is simultaneously passed to the 'write surface reflectance IP' routine and to the BRDF-coupling adjustment subroutine. Some land quality (LQ) flags may be required during processing within the BRDF-coupling subroutine. The output of the BRDF-coupling adjustment routine is then passed to the 'write surface reflectance IP'.

3.2 ALGORITHM INPUT

3.2.1 VIIRS Data

The Surface Reflectance IP algorithm uses the following VIIRS data:

- VIIRS Aerosol Optical Thickness IP [Y2388]
- VIIRS Precipitable Water IP (fallback water vapor source if it becomes available over land) [Y3251]
- VIIRS 375-m Earth View SDR (including radiances, geometry, geolocation, and elevation for bands I1, I2, and I3) [Y3261]
- VIIRS 750-m Earth View SDR (including radiances, geometry, geolocation, and elevation for bands M1, M2, M3, M4, M5, M7, M8, M10, and M11) [Y3261]. The VIIRS M9 band is used for the cirrus correction.
- VIIRS Cloud Mask IP (including cloud and land/water mask) [Y2412]
- Surface Reflectance LUTs based on VIIRS spectral response curves

3.2.2 Non-VIIRS Data

The Surface Reflectance IP algorithm uses the following non-VIIRS data:

- Surface Pressure from National Center for Environmental Prediction (NCEP), or Navy Operational Global Atmospheric Prediction System (NOGAPS) analyses, or a digital elevation map, such as the GTOPO05 from the EDC, USGS as a graceful degradation scheme.

- Precipitable Water from NCEP or NOGAPS analyses
- Column Ozone from NCEP or NOGAPS analyses
- Column Ozone from Ozone Mapping Profiling Suite (OMPS, fallback ozone source)

3.3 ALGORITHM OUTPUT

The Surface Reflectance IP algorithm output (i.e., write surface reflectance IP) consists of the following:

1. Solar/Viewing Geometry parameters (solar zenith angle, viewing zenith angle, relative azimuth, pixel elevation above sea level)
2. Quality Flags
3. Surface reflectance retrieved assuming a lambertian surface
4. Surface reflectance from (3) adjusted for adjacency effects
5. Surface reflectance from (4) adjusted for adjacency effects and BRDF coupling effects

3.4 THEORETICAL DESCRIPTION—PHYSICS AND MATHEMATICAL BACKGROUND

3.4.1. Introduction

The retrieval of surface reflectance from electro-optical spectral sensors usually requires calibrating the sensor input to reflectance units, and removing the relatively small contribution due to the atmosphere. The principal atmospheric components affecting the top-of-atmosphere (TOA), or at-satellite-reflectance in the range of 0.4-2.5 μm are shown in Figure 7.

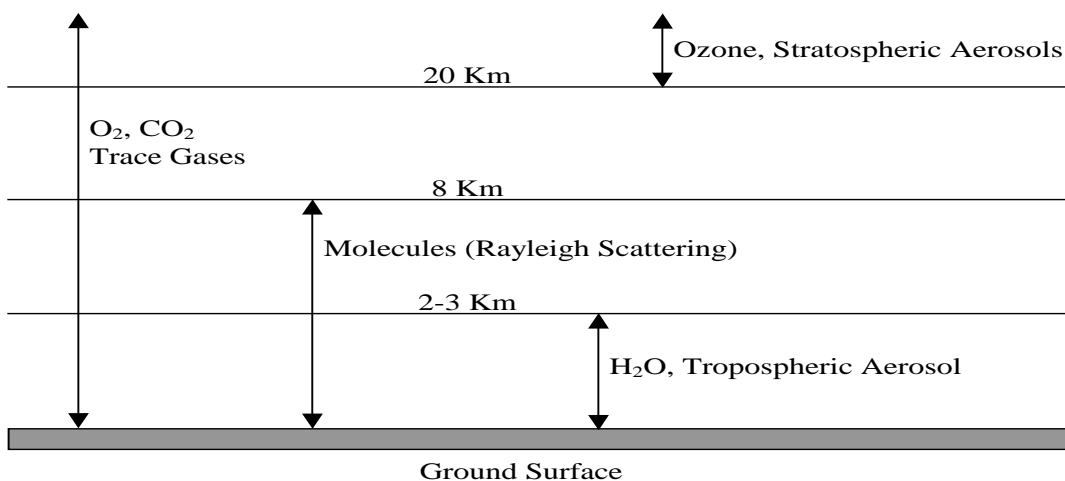


Figure 7. The atmospheric components affecting the remote sensing signal in the 0.4-2.5 μm range.**3.4.2 Lambertian correction****3.4.2.1 Formalism**

Using the formalism developed for the 6S code, the solution of the radiation transfer equation employing the Lambertian Uniform Target assumption for observation in electro-optical spectral band i , assuming a standard atmospheric profile, but variable ozone and water vapor amount, is written as (Vermote *et al.*, 1997):

$$\rho_{TOA}^i(\theta_s, \theta_v, \phi, P, Aer^i, U_{H_2O}, U_{O_3}) = Tg_{OG}^i(m, P)Tg_{O_3}^i(m, U_{U_{O_3}})[\rho_{atm}^i(\theta_s, \theta_v, \phi, P, Aer^i, U_{H_2O}) + Tr_{atm}^i(\theta_s, \theta_v, P, Aer^i) \frac{\rho_s}{1 - S_{atm}^i(P, Aer^i)} Tg_{H_2O}^i(m, U_{H_2O})] \quad (1)$$

$$Aer^i = (\tau_A^i, \omega_0^i, P_A^i)$$

where (dropping the spectral dependence i)

ρ_{TOA} is the reflectance at the top of the atmosphere,

Tg is the gaseous transmittance by water vapor, Tg_{H_2O} , by ozone, Tg_{O_3} , or other gases, Tg_{OG} (e.g. CO_2 , O_2 , CH_4)

Aer refers to the aerosol model optical properties,

ρ_{atm} is the atmosphere intrinsic reflectance,

Tr_{atm} is the total atmosphere transmission (downward and upward)

S_{atm} is the atmosphere spherical albedo,

ρ_s is the surface reflectance to be retrieved by the atmospheric correction procedure,

The geometrical conditions are given by θ_s , the solar zenith angle, θ_v , the view zenith angle and ϕ , the difference between the solar and view azimuth angle,

P is the pressure in Millibars, which influences the amount of molecules in the atmosphere and the concentration of absorbing gases,

τ_A , ω_0 and P_A describe the aerosol properties in band i .

τ_A is the spectral aerosol optical thickness,

ω_0 is the spectral aerosol single scattering albedo, describing the absorption of the aerosol, ω_0 is equal to 1 for non-absorption particles and to 0 for completely absorbing aerosol,

P_A is the spectral aerosol phase function,

U_{H_2O} is the integrated water vapor content in centimeters

U_{O_3} is the integrated columnar ozone content in cm-atm
m is the air-mass computed as $1/\cos(\theta_s)+1/\cos(\theta_v)$

The water vapor affect on the atmosphere intrinsic reflectance is approximated in 6S as:

$$\rho_{atm}^i(\theta_s, \theta_v, \phi, P, Aer^i, U_{H_2O}) = \rho_R^i(\theta_s, \theta_v, \phi, P) + (\rho_{R+Aer}^i(\theta_s, \theta_v, \phi, P, Aer^i) - \rho_R^i(\theta_s, \theta_v, \phi, P)) T_{g_{H_2O}}^i(m, \frac{U_{H_2O}}{2}) \quad (2)$$

where ρ_R represents the atmospheric reflectance due to molecular (Rayleigh) scattering, and ρ_{R+Aer} represents the reflectance of the combined molecular and aerosol components, which is computed in 6S using the successive order of scattering method, and thereby accounting correctly for the so-called coupling effect (Deschamps *et al.*, 1983). This approximation conserves the correct computation of the coupling, and supposes that the water vapor is mixed with aerosol and that the molecular scattering is not affected by the water vapor absorption. This approximation is reasonable in most cases where observation bands are narrow and outside the water vapor strong absorption as it is the case for VIIRS or MODIS.

The total atmosphere transmission, T_r , is further decomposed into downward and upward terms, which are respectively dependent on θ_s and θ_v and are computed using the same function by virtue of the reciprocity principle, that is:

$$T_{atm}^i(\theta_s, \theta_v, P, Aer^i) = T_{atm}^i(\theta_s, P, Aer^i) T_{atm}^i(\theta_v, P, Aer^i) \quad (3)$$

3.4.2.2 Lambertian infinite target correction implementation

In the implementation of the algorithm, functions related to atmospheric scattering and absorption, ρ_{atm} , T_{atm} and S_{atm} are interpolated from pre-computed look up table since they cannot be simply modeled. On the other hand, the gaseous transmission functions can be written as simple analytical expressions. The molecular reflectance term can be computed very efficiently using a semi-empirical approach based on the decomposition suggested by Chandrasekhar.

Using the approximation given below in (4), the dependence on the atmospheric pressure can be accounted for, by only computing ρ_{R+Aer} at standard pressure, P_0 , which substantially reduces the dimension of the look-up tables. We use:

$$\rho_{am}^i(\theta_s, \theta_v, \phi, P, Aer^i, U_{H_2O}) = \rho_R^i(\theta_s, \theta_v, \phi, P) + \left(\rho_{R+Aer}^i(\theta_s, \theta_v, \phi, P_0, Aer^i) - \rho_R^i(\theta_s, \theta_v, \phi, P_0) \right) Tg_{H_2O}^i\left(m, \frac{U_{H_2O}}{2}\right) \quad (4)$$

A similar approach is applied to the atmospheric transmission term, that is:

$$T_{am}^i(\theta, P, Aer^i) = T_{am}^i(\theta, P_0, Aer^i) \frac{T_R^i(\theta, P)}{T_R^i(\theta, P_0)} \quad (5)$$

where T_R is the atmosphere transmission function due to molecule.

3.4.2.3 Lambertian infinite target correction operational approach

The code implements Equations (1) through (5), using a look-up table approach and analytic expressions. The following section details the computation of each term in the computer code.

3.4.2.3.1 Gaseous transmission by other gases

The gaseous transmission by gases, other than water vapor or ozone, $Tg_{OG}^i(m, P)$, in the VIIRS bands can be written as a function of the air mass, m , and the pressure P (in atm), as follows:

$$Tg_{OG}^i(m, P) = \exp\left[m(a_0^i P + a_1^i \text{Log}(P)) + \text{Log}(m)(b_0^i P + b_1^i \text{Log}(P)) + m \text{Log}(m)(c_0^i P + c_1^i \text{Log}(P))\right] \quad (6)$$

3.4.2.3.2 Ozone Gaseous transmission

The ozone gaseous transmission, $Tg_{O_3}^i(m, U_{O_3})$, in the narrow VIIRS bands (i.e., in the Chappuis band) could be simply modeled as:

$$Tg_{O_3}^i(m, U_{O_3}) = e^{-ma_{O_3}^i U_{O_3}} \quad (7)$$

The coefficients $a_{O_3}^i$ are determined by curve fitting. The units of U_{O_3} are cm-atm.

3.4.2.3.3 Water vapor Gaseous transmission

The water vapor transmission, $Tg_{H_2O}^i(m, U_{H_2O})$, is modeled as:

$$Tg_{H_2O}^i(m, U_{H_2O}) = \exp\left[a_{H_2O}^i m U_{H_2O} + b_{H_2O}^i \text{Log}(m U_{H_2O}) + c_{H_2O}^i m U_{H_2O} \text{Log}(m U_{H_2O})\right] \quad (8)$$

The coefficients $a_{H_2O}^i$, $b_{H_2O}^i$ and $c_{H_2O}^i$ are determined by curve fitting.

3.4.2.3.4 Molecular atmospheric reflectance at standard pressure

The molecular atmospheric reflectance at standard pressure, $\rho_R^i(\theta_s, \theta_v, \phi, P_0)$, is computed by the subroutine CHAND.f, which takes as input, the geometry (μ_s, μ_v, Φ), where μ_s (resp. μ_v) is the cosine of the solar (resp. view) zenith angle, and Φ the relative azimuth and the molecular optical thickness in that case at standard pressure, which is pre-computed (by 6S), τ_R .

3.4.2.3.5 Molecular atmospheric reflectance at actual pressure

The molecular atmospheric reflectance at actual pressure adjustment, $\rho_R^i(\theta_s, \theta_v, \phi, P)$, is simply done by adjusting the amount of molecule or the molecular optical thickness, according to:

$$\tau_R(P) = P \tau_R \quad (9)$$

where the pressure P is expressed in atmospheres.

3.4.2.3.6 Intrinsic reflectance at standard pressure

The intrinsic atmospheric reflectance at standard pressure, $\rho_{R+Aer}^i(\theta_s, \theta_v, \phi, P_0, Aer^i)$, is pre-computed by 6S in a look table for each band and each aerosol model (P_A, ω_{\square}). The step in solar zenith angle is 4 deg, in view angle is 4 deg corresponding to the gauss quadrature of 24 angles (with the nadir added), the step is kept constant in scattering angle (4 degree), Θ_{\square} which is defined as:

$$\cos(\Theta) = -\cos(\theta_s) \cos(\theta_v) - \cos(\phi) \sin(\theta_s) \sin(\theta_v), \quad (10)$$

resulting in a variable number of steps for each θ_s, θ_v configuration. The indexing to the correct values in the look up table is achieved through the use of the ANGLE lookup table, which keeps track of the number of geometry computed for each θ_s, θ_v configuration. Though, more expensive and more complicated to interpolate within, this structure achieves a higher precision with a reduced size look up table, for a term whose accuracy is critical to the atmospheric correction.

The step in aerosol optical depth is variable to optimize the performance of the correction with the error induced by the interpolation (i.e. finer a low optical depth).

3.4.2.3.7 Atmospheric transmission on at standard pressure

Atmospheric transmission, $T_{atm}^i(\theta, P_0, Aer^i)$, is pre-computed using 6S, with the successive order of scattering method assuming the bottom of the layer is illuminated with isotropic light. The code accounts for the mixing aerosol molecule within the atmosphere. The values are computed with a step of 4 deg in θ and for each aerosol model and each band for the

predefined values of τ_A . The interpolation for any θ and τ is relatively straightforward since this table has only 2 dimensions. The table volume is also very modest.

3.4.2.3.8 Molecular (Rayleigh) transmission at standard pressure

The molecular transmission, $T_R^i(\theta, P_0)$, at standard pressure is computed using the value of molecular optical depth at standard pressure, τ_R . Using the two stream method, the molecular transmission is approximated by:

$$T_R^i(\theta, P_0) = \frac{\left[\frac{2}{3} + \cos(\theta) \right] + \left[\frac{2}{3} - \cos(\theta) \right] e^{-\tau_R / \cos(\theta)}}{\frac{4}{3} + \tau_R} \quad (11)$$

3.4.2.3.9 Molecular (Rayleigh) transmission at actual pressure.

The Rayleigh transmission, $T_R^i(\theta, P)$, determination uses the same method as in Section 3.4.2.3.5 we simply replace τ_R in Equation (9) with $\tau_R(P)$.

3.4.2.3.10 Atmosphere spherical albedo at actual pressure

The atmospheric spherical albedo at actual pressure, $S_{atm}^i(P, Aer^i)$, is defined as:

$$S_{atm}^i(P, Aer^i) = \int_0^{\pi/2} \int_0^{\pi} \int_0^{2\pi} \rho_{atm}^i(\theta, \theta', \phi, P, Aer^i) \sin(\theta) \cos(\theta') d\theta d\theta' d\phi \quad (12)$$

By ignoring the water vapor dependence on the atmosphere intrinsic reflectance (S acting as a second order effect), we can write the same relation we have written for the atmosphere intrinsic reflectance, that is

$$S_{atm}^i(P, Aer^i) = (S_{atm}^i(P_0, Aer^i) - S_R^i(P_0)) + S_R^i(P) \quad (13)$$

So the $S_{atm}^i(P_0, Aer^i)$ is stored in a pre-calculated look up table depending only on aerosol optical depth and model. The $S_R^i(P)$ term is computed by an analytic expression based on the integral of Equation (11) that is:

$$S_R^i(P) = \sum_j a_j EXPI(\tau_R, n), \quad (14)$$

where EXPI is the exponential integral function (see 6S code for details; Vermote et al., 1994).

3.4.3 Adjacency Adjustment

3.4.3.1 Formalism

If the target is of infinite dimension, the equation of transfer (here rewritten without gaseous absorption to simplify the writing), and dropping the spectral dependence then:

$$\rho_{toa} = \rho_{R+Aer} + \frac{T_{R+Aer}(\theta_s)T_{R+Aer}(\theta_v)\rho_s}{1 - S_{R+Aer}\rho_s} \quad (15)$$

In the case where the target is not infinite, Equation (15) becomes:

$$\rho_{toa} = \rho_{R+Aer} + \frac{T_{R+Aer}(\theta_s)}{1 - S_{R+Aer}\rho_e} \left(e^{-\tau/\mu_v} \rho_s + t_{R+Aer}^d(\theta_v)\rho_e \right) \quad (16)$$

$$\rho_e = \frac{1}{2\pi} \int_0^{2\pi} \int_0^\infty \rho(r, \psi) \frac{dF(r)}{dr} dr d\psi \quad (17a)$$

In Equation (16), the downward transmission, $T_{R+Aer}(\theta_s)$, where θ_s refers to the solar zenith angle, and the upward transmission, $T_{R+Aer}(\theta_v)$, where θ_v refers to view zenith angle are considered separately. Furthermore, the upward transmission term, $T_{R+Aer}(\theta_v)$, is decomposed into two parts: (a) the diffuse upward transmission $t_{R+Aer}^d(\theta_v)$, and (b) the direct upward transmission ($e^{-\tau/\mu_v}$), (where μ_v refers to the cosine of the view zenith angle and τ refers to the atmosphere optical thickness). In extenso, we have

$$T_{R+Aer}(\theta) = t_{R+Aer}^d(\theta) + e^{-\tau_{R+A}/\mu} \quad (17b)$$

By decomposing the signal in this way the contribution coming directly from the target the term ($e^{-\tau/\mu_v} \rho_s$) is isolated from the “environment contribution”, ρ_e , coming from adjacent pixels not in the direct line of sight. The adjacent pixels contribute to the signal due to the atmospheric scattering of the photons toward the sensor and their contribution is therefore weighted by the diffuse upward transmission.

The effective “reflectance” of the environment, ρ_e , is not a simple average of the pixel around the target but is the result of the convolution of the atmospheric point spread function $dF(r)/dr$ by the two dimensional surface reflectance values. In Equation (17), the spatial coordinate system used is the polar coordinate system (r for radius, Ψ for angle), which is very convenient since in most cases the point spread function is only dependent the distanced from the target and not the angle. In practice the dependence with respect to Ψ is actually dropped.

The atmospheric point spread functions for molecules and aerosols have been computed using Monte-Carlo computation and fitted using empirical functions and are available in the 6S

code (Vermote et al., 1997). Figure 8 shows the environment function for molecules and aerosols as a function of the distance from the target center for nadir viewing condition and for a sensor located at the top of the atmosphere. In the aerosol case, the contribution of the environment decreases quickly with distance. In the case of molecules, scattering is more important, the contribution of the environment varies more slowly, and the impact of the environment can be seen at larger distances. It is worth pointing out that these environment functions will vary as a function of view angle and altitude of the sensor within the atmosphere (Vermote et al., 1997), and also, to a certain extent, will depend on the aerosol type (especially their vertical profile).

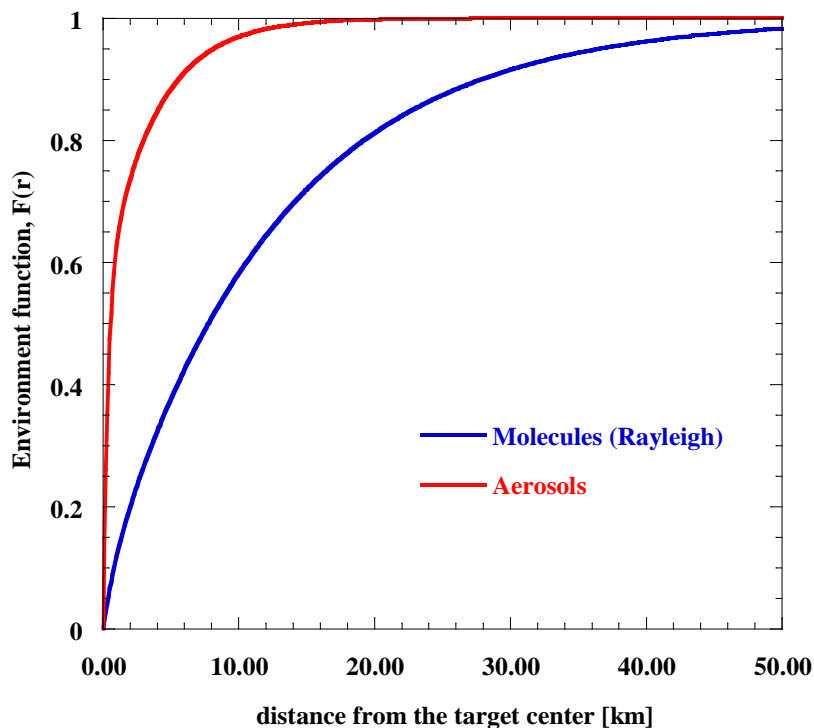


Figure 8: Atmospheric environment function as a function of the distance from the target center, for molecules and aerosols.

In practice, the atmosphere environment function, $F(r)$, is computed by a weighting average of the individual molecules and aerosol environment functions using their respective upward diffuse transmissions, ($t_d^R(\theta_v)$ and $t_d^{Aer}(\theta_v)$), that is:

$$F(r) = \frac{t_d^R(\theta_v)F^R(r) + t_d^{Aer}(\theta_v)F^A(r)}{t_d^{R+Aer}(\theta_v)} \quad (18)$$

3.4.3.2 Correction for adjacency effect-implementation

In the Lambertian approximation, Equation (15) shows that the surface reflectance, ρ_{Lamb} can be retrieved in two simple steps given in Equation (19a) and (19b):

$$\gamma = \frac{\rho_{toa} - \rho_{R+Aer}}{T_{R+Aer}(\theta_s)T_{R+Aer}(\theta_v)} \quad (19a)$$

$$\rho_{Lamb} = \frac{\gamma}{1 + S_{R+Aer}\gamma} \quad (19b)$$

If the target is not of infinite radius then the result of Equation (19a), becomes,

$$\gamma = \frac{\rho_s e^{-\tau/\mu_v} + t_{R+Aer}^d(\theta_v)\rho_e}{T_{R+Aer}(\theta_v)(1 - S_{R+Aer}\rho_e)} \quad (20)$$

which can easily be solved for ρ_s :

$$\rho_s = [\gamma T_{R+Aer}(\theta_v)(1 - S_{R+Aer}\rho_e) - t_{R+Aer}^d(\theta_v)\rho_e] / e^{-\tau/\mu_v} \quad (21)$$

Since the Lambertian surface reflectance is computed before the adjacency correction (an average of the Lambertian correction is needed in the adjacency correction) ρ_{Lamb} can be used instead of γ to compute ρ_s . This results in the following correction formula:

$$\rho_s = \left[\frac{(1 - S_{R+Aer}\rho_e)}{(1 - S_{R+Aer}\rho_{Lamb})} T_{R+Aer}(\theta_v)\rho_{Lamb} - t_{R+Aer}^d(\theta_v)\rho_e \right] / e^{-\tau/\mu_v} \quad (22)$$

To compute ρ_e it is necessary to convolve the atmospheric point spread function with the two dimensional surface reflectance according to Equation (17a). The actual surface reflectance at a very fine scale level is usually not available; instead the actual measurements can be used. An approximation for Equation (17) (Putsay, 1992) is:

$$\rho_e = \sum_{j=-n}^n \sum_{i=-n}^n \frac{dF(r(i,j))}{dr} \rho_{Lamb}(i,j) \quad (23)$$

In Equation (23), the pixels of the image itself are used to compute the background reflectance, therefore the average point spread function at the pixel location (i,j) is used. The second approximation is that the estimate of the surface reflectance at location (i,j) using the infinite radius target approximation is used instead of the actual reflectance. That provides a

first guess for the environment contribution that may actually be refined by successive iterations, but those iterations are usually not necessary (Putsay, 1992).

This first guess is based on the order of tens to hundreds of pixels, which according to the MODIS surface reflectance ATBD corresponds to an n between 3 and 10. In practice, the contribution from the environment encompasses the pixels within 1200 m of the center pixel. The VIIRS algorithm uses $n=3$ for the imagery band values and $n=2$ for the moderate resolution band values.

3.4.3.3 Correction for adjacency effect-operational approach

Most of the term described in Equations (19) to (22) are already in look up table. The additional look up table that needs to be provided is the computation of the optical thickness at the given wavelength, τ_{R+A} , used to compute the direct transmission term, $e^{-\tau_{R+A}/\mu_v}$, this optical thickness, $\tau_{R+A}=\tau_A+\tau_R$ is computed from the spectral extinction coefficient stored in the spherical albedo look up table to compute τ_A and the molecular optical thickness τ_R . The atmospheric point spread function is also stored as a look up table for the Rayleigh, $dF_R(r)/dr$ and aerosol contribution $dF_A(r)/dr$.

3.4.4 BRDF atmosphere coupling correction

3.4.4.1 Formalism

Equation (15) assumed that the target is lambertian, if we account for the fact that it is not a lambertian reflector, Equation (15) can be written as (Vermote, 1997)

$$\rho_{toa}(\mu_s, \mu_v, \phi) = \rho_{R+Aer}(\mu_s, \mu_v, \phi) + e^{-\tau/\mu_s} e^{-\tau/\mu_v} \rho_s(\mu_s, \mu_v, \phi) + e^{-\tau/\mu_s} t_d(\mu_s) \bar{\rho}_s + e^{-\tau/\mu_s} t_d(\mu_v) \bar{\rho}'_s + t_d(\mu_v) t_d(\mu_s) \bar{\bar{\rho}}_s + \frac{T_{R+Aer}(\mu_s) T_{R+Aer}(\mu_v) S_{R+A}(\bar{\bar{\rho}}_s)^2}{1 - S_{R+Aer} \bar{\bar{\rho}}_s} \quad (23a)$$

with μ_s (resp. μ_v) the cosine of the sun (resp. view) zenith angle, ϕ the relative azimuth (sun – view), $\bar{\rho}_s$, $\bar{\rho}'_s$, and $\bar{\bar{\rho}}_s$ the term accounting for the coupling between the atmosphere and the surface BRDF, if the target is lambertian then $\bar{\rho}_s = \bar{\rho}'_s = \bar{\bar{\rho}}_s = \bar{\rho}_s$; otherwise we have:

$$\bar{\rho}_s(\mu_s, \mu_v, \phi) = \frac{\int_0^{2\pi} \int_0^1 \mu L_{R+A}^\downarrow(\mu_s, \mu, \phi') \rho_s(\mu, \mu_v, \phi' - \phi) d\mu d\phi'}{\int_0^{2\pi} \int_0^1 \mu L_{R+A}^\downarrow(\mu_s, \mu, \phi') d\mu d\phi'} \quad (23b)$$

$$\bar{\rho}'_s(\mu_s, \mu_v, \phi) = \bar{\rho}_s(\mu_v, \mu_s, \phi) \quad (23c)$$

$$\bar{\bar{\rho}}_s(\mu_s, \mu_v, \phi) = \bar{\rho}'_s(\mu_s, \mu_v, \phi) \quad (23d)$$

Where $L_{R+A}^{\downarrow}(\mu_s, \mu, \phi')$ is the downwelling flux.

Equation (23d) is approximated like the spherical albedo or white sky albedo, namely:

$$\bar{\bar{\rho}}_s \equiv \int_0^1 \int_0^{2\pi} \int_0^1 \mu \rho_s(\mu, \mu, \phi' - \phi) d\mu d\phi' d\mu' \quad (23e)$$

3.4.4.2 BRDF atmosphere coupling correction Implementation

The BRDF of the target, $\rho_s(\mu, \mu', \phi')$ is in general unknown for any geometrical condition for the purpose of atmospheric correction. However, we will assume that the BRDF shape can be determined a priori. This simplifying assumption is necessary since Equation (23a) shows that the Top of the Atmosphere reflectance is given in terms of integrals of the BRDF of the surface Equations (23b-e). In other words Equation (23a) is a non-linear integral equation for the BRDF function. Solving this equation rigorously in an operational setting is prohibitive since it would require multiple iterations of a radiative transfer model.

The unknown reflectance is the line of sight reflectance $\rho_s(\mu_s, \mu_v, \phi)$ but the BRDF of the target $\rho_s(\mu, \mu', \phi')$ is assumed to satisfy:

$$\rho_s(\mu, \mu', \phi') = \rho_s(\mu_s, \mu_v, \phi) \frac{\rho_m(\mu, \mu', \phi')}{\rho_m(\mu_s, \mu_v, \phi)} \quad (24)$$

Where $\rho_m(\mu, \mu', \phi')$ is the “modeled” BRDF and the ratio $\frac{\rho_m(\mu, \mu', \phi')}{\rho_m(\mu_s, \mu_v, \phi)}$ is the BRDF shape.

Using that assumption, Equation (23b) can be rewritten as:

$$\bar{\rho}_s(\mu_s, \mu_v, \phi) = \frac{\rho_s(\mu_s, \mu_v, \phi)}{\rho_m(\mu_s, \mu_v, \phi)} \bar{\rho}_m(\mu_s, \mu_v, \phi) = \rho_s(\mu_s, \mu_v, \phi) \bar{\rho}_m^{shape}(\mu_s, \mu_v, \phi) \quad (24b)$$

And similarly for Equations (23c) and (23e):

$$\bar{\rho}_s^{\uparrow}(\mu_s, \mu_v, \phi) = \frac{\rho_s(\mu_s, \mu_v, \phi)}{\rho_m(\mu_s, \mu_v, \phi)} \bar{\rho}_m^{\uparrow}(\mu_s, \mu_v, \phi) = \rho_s(\mu_s, \mu_v, \phi) \bar{\rho}_m^{\uparrow shape}(\mu_s, \mu_v, \phi) \quad (24c)$$

$$\bar{\bar{\rho}}_s \equiv \frac{\rho_s(\mu_s, \mu_v, \phi)}{\rho_m(\mu_s, \mu_v, \phi)} \int_0^1 \int_0^{2\pi} \int_0^1 \mu \rho_m(\mu, \mu', \phi' - \phi) d\mu d\phi' d\mu' = \rho_s(\mu_s, \mu_v, \phi) \bar{\bar{\rho}}_m^{shape}(\mu_s, \mu_v, \phi) \quad (24e)$$

So Equation (23a) is written as:

$$\begin{aligned} \rho_{toa}(\mu_s, \mu_v, \phi) = & \rho_{R+Aer}(\mu_s, \mu_v, \phi) + \rho_s(\mu_s, \mu_v, \phi) [e^{-\tau/\mu_s} e^{-\tau/\mu_v} + e^{-\tau/\mu_s} t_d(\mu_v) \overline{\rho}_m^{shape} \\ & + e^{-\tau/\mu_s} t_d(\mu_v) \overline{\rho}_m^{shape} + t_d(\mu_v) t_d(\mu_s) \overline{\rho}_m^{shape}] + \rho_s(\mu_s, \mu_v, \phi)^2 \frac{T_{R+Aer}(\mu_s) T_{R+Aer}(\mu_v) S_{R+Aer} \overline{\rho}_m^{shape}}{1 - S_{R+Aer} \overline{\rho}_m^{shape}} \end{aligned} \quad (25)$$

Equation (25) is a quadratic equation in $\rho_s(\mu_s, \mu_v, \phi)$ that has only one positive solution, since the product of the roots is negative. Therefore solving for $\rho_s(\mu_s, \mu_v, \phi)$ is straightforward once each other term of Equation (25) is computed. The computation of $\overline{\rho}_m^{shape}$, $\overline{\rho}_m^{shape}$ and $\overline{\rho}_m^{shape}$, which are the only quantities not fully defined in the previous section, is described in the operational approach (next section).

3.4.4.3 BRDF atmosphere coupling correction-operational approach

The model of BRDF used for $\rho_m(\mu, \mu', \phi')$ is the operational model used for MODIS Albedo/BRDF product the LiSparse-Reciprocal (LSR), RossThick (RT) linear kernel model that is written as:

$$\rho_m(\mu_s, \mu_v, \phi) = P_1 + P_2 K_{LSR}(\mu_s, \mu_v, \phi) + P_3 K_{RT}(\mu_s, \mu_v, \phi) \quad (26)$$

where

$$K_{RT}(\mu_s, \mu_v, \phi) = \frac{(\pi/2 - \xi) \cos \xi + \sin \xi}{\mu_s + \mu_v} - \frac{\pi}{4}$$

$$\cos \xi = \mu_s \mu_v + \sqrt{1 - \mu_s^2} \sqrt{1 - \mu_v^2} \cos \phi$$

$$K_{LSR}(\mu_s, \mu_v, \phi) = O(\mu_s, \mu_v, \phi) - \frac{1}{\mu_s} - \frac{1}{\mu_v} + \frac{1}{2}(1 + \cos \xi) \frac{1}{\mu_s} \frac{1}{\mu_v}$$

$$O(\mu_s, \mu_v, \phi) = \frac{1}{\pi} (t - \sin t \cos t) \left(\frac{1}{\mu_s} + \frac{1}{\mu_v} \right)$$

$$\cos t = \frac{h}{b} \frac{\sqrt{D^2 + (\tan \theta' \tan \vartheta' \sin \phi)^2}}{\sec \theta' + \sec \vartheta'}$$

$$D = \sqrt{\tan^2 \theta' + \tan^2 \vartheta' - 2 \tan \theta' \tan \vartheta' \cos \phi}$$

$$\theta' = \tan^{-1} \left(\frac{b}{r} \tan \theta_s \right) \quad \vartheta' = \tan^{-1} \left(\frac{b}{r} \tan \vartheta_v \right)$$

where, h describes the crown model central height above the ground, r and b describe the vertical and horizontal dimensions of the crown spheroid.

The interesting properties of this BRDF model are that the geometrical conditions are decoupled from the surface weighting parameters, therefore:

$$\bar{\rho}_m^{shape}(\mu_s, \mu_v, \phi) = \frac{1 + \frac{P_2}{P_1} \bar{K}_{LSR}(\mu_s, \mu_v, \phi) + \frac{P_3}{P_1} \bar{K}_{RT}(\mu_s, \mu_v, \phi)}{1 + \frac{P_2}{P_1} K_{LSR}(\mu_s, \mu_v, \phi) + \frac{P_3}{P_1} K_{RT}(\mu_s, \mu_v, \phi)} \quad (27)$$

So by pre-computing the downward irradiance integrals $\bar{K}_{LSR}(\mu_s, \mu_v, \phi)$ and $\bar{K}_{RT}(\mu_s, \mu_v, \phi)$ for the kernels, $K_{LSR}(\mu_s, \mu_v, \phi)$ and $K_{RT}(\mu_s, \mu_v, \phi)$ storing them in look up tables (they are function of the band i , the optical thickness at 550nm, and the aerosol model), the functions

$\bar{\rho}_m^{shape}(\mu_s, \mu_v, \phi)$ and their associate ($\bar{\rho}_m^{shape}(\mu_s, \mu_v, \phi)$ and $\overline{\rho}_m^{shape}$) can be recomputed on the fly.

The only unknown at this point is the weight of the BRDF shape function, $P_2' = \frac{P_2}{P_1}$ and $P_3' = \frac{P_3}{P_1}$

Some experiments with MODIS data have shown that the BRDF shape parameter can be fitted as a function of NDVI. That is, to a first order, for low NDVI, low vegetation cover, P_2' and P_3' are expected to be near zero since the BDRF effect are small, for higher NDVI, the coefficient are expected to be higher. It should be noted, that P_2' and P_3' depend on the band as well. In the present version of the code, a linear interpolation is performed between a semi-arid case (low NDVI) and a forest case (high NDVI) for which the P_2' are P_3' have inverted using as large a data record as possible. Figure 9, shows the coefficients. P_2' (Li Sparse Reciprocal) and P_3' (Ross Thick) for three different biomass cases (low, average, high) for each of the VIIRS bands.

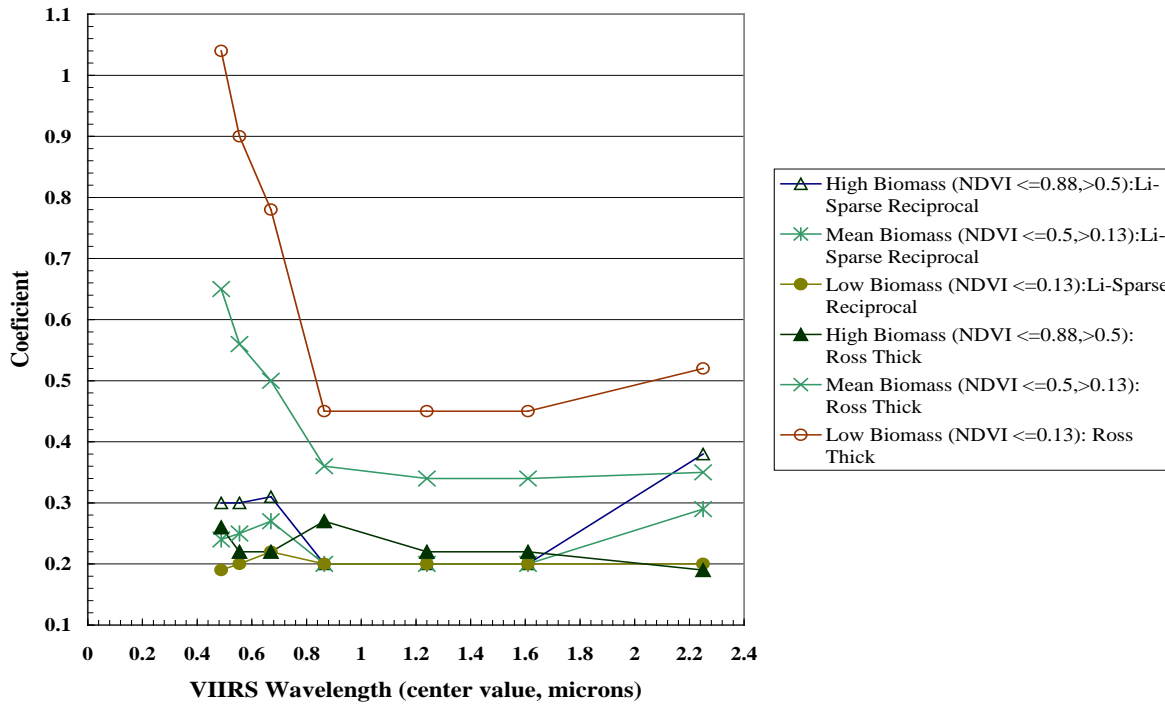


Figure 9. Relationship between BRDF shape and NDVI.

3.4.5 Thin Cirrus Correction

Should thin cirrus (presently defined to possess optical thickness at 640 nm ranging up to 1) be present, the Surface Reflectance IP and downstream products are generated, with an associated flag in the Land Quality Flag output. The baseline approach for removing much of the thin cirrus-laden pixels is very simple. It assumes that cirrus reflectance is not spectrally dependent, and that cirrus reflectance is spatially homogeneous. This allows the application of a threshold adjustment to all VIIRS bands in the general form

$$\rho_{\lambda} = \rho_{1.38} - (\rho_{1.38} / T_{H2O}^{1.38}) \quad (28)$$

where ρ_{λ} is the reflectance at the particular band, $\rho_{1.38}$ is the reflectance at the 1.38 micron VIIRS band, and $T_{H2O}^{1.38}$ is the total two-way transmittance of water vapor at 1.38 microns for the given solar and viewing geometry. $T_{H2O}^{1.38}$ is assumed to be 0.6, based on Vermote and Vermeulen (1999).

This correction will be applied to the radiances in the other VIIRS reflective bands prior to the application of the lambertian correction. The inherent assumption within Equation (16), even at VIIRS scale, may not be valid under every circumstance, but suspected pixels are nonetheless flagged. A few reasons why the assumption might not be valid include, cirrus ice

crystals are not spatially homogeneous, and cirrus adjacency issues. Vermote and Vermeulen (1999) provide additional insights.

3.5 ALGORITHM VERIFICATION

The Surface Reflectance IP algorithm performance may be affected by sensor, solar and viewing geometry including target elevation above sea level, atmospheric, adjacency, and coupling of the atmosphere and surface effects, i.e. BRDF, among others. The atmospheric effects include aerosol and Rayleigh scattering, gaseous absorption, and thermodynamic conditions. The largest atmospheric effects on surface reflectance retrieval are from variations in aerosol properties. Sensor calibration is the primary contributor to sensor effects. The effect of variations of input parameters on the surface reflectance calculated assuming a lambertian surface (ρ_λ (lamb)), surface reflectance assuming a lambertian surface but adjusting for adjacency (ρ_λ (adj)), as well as surface reflectance assuming a lambertian surface, adjusted for adjacency, and BRDF-coupling (ρ_λ (BRDF)) can not be investigated in detail until we obtain final sensor calibration curves, and additional vicarious calibration data cubes. Meanwhile a preliminary verification of the algorithm was performed on 2 scenes, and the results for a couple points within each scene are presented.

DERIVED REQUIREMENTS:

There are no explicit quality requirements on the Surface Reflectance IP in the VIIRS SRD. We have, however, derived performance requirements for surface reflectance retrievals to assist in the interpretation of our algorithm sensitivity tests. The requirements for surface reflectance are primarily derived from the specification requirements placed on the Vegetation Index Environmental Data Record (EDR), and the Surface Albedo EDR. The Surface Albedo EDR requires that the surface reflectance values be retrieved to within 0.05 of an albedo unit. For example, Liang et al. (2002) showed that when the surface reflectance values (derived from MODIS products) were within 5% absolute error, the resulting broadband albedo values had an absolute error within 2%. The Vegetation Index EDR has two general components, the Normalized Difference Vegetation Index (NDVI) and the Enhanced Vegetation Index (EVI). The implied specification on the top of canopy (TOC) EVI requires that in the most stringent case the VIIRS surface reflectance values be retrieved to within 0.012 of a surface reflectance unit. This would be sufficient to meet the specification on EVI but it is not necessary.

The absolute error in the retrieved surface reflectance assuming a lambertian surface is typically 0.02 to 0.06 of a unit for a clear atmosphere to 0.03-0.11 for a hazy atmosphere (aerosol optical thickness of 0.5) at a solar zenith angle of 60 degrees and at the maximum backscattering point (i.e., at the hot spot). Thus, in order to meet the system specification set for the vegetation index as well as the surface albedo, further adjustments are likely to be necessary. Lyapustin (2001) showed that as much as 0.04 – 0.06 absolute differences in the near infrared and 0.01-0.04 of a reflectance unit in the visible spectral range at a 25 m spatial resolution could be accounted for as the radiative contribution from surrounding pixels (not predominantly from the atmosphere), i.e., adjusting for adjacency effects. Adjacency adjustments are typically within 0.005 and 0.02 reflectance units at 1 km resolution. The

assumption of a lambertian surface could contribute 0.02 – 0.06 reflectance units absolute difference (compared to true reflectance).

The current lack of sufficient data and final spectral response functions for VIIRS mandates that we perform a preliminary verification investigation of the VIIRS output against the corresponding output from MODIS despite their spectral and spatial differences. The result of this investigation requires a close agreement with the MODIS heritage sensor data, particularly in the VIIRS M4 and MODIS band 4 spectral region, where the spectral differences between the two sensors are minimal, in order for this algorithm to have a chance of meeting the derived requirements.

3.5.1 Preliminary Verification Test

This sub-section shows that the results from this code compare favorably to corresponding MODIS output for two scenes: i) Arizona Scene, and ii) Amazon Scene. Further, the results of this test do not preclude future tests due to code enhancements, such as updated spectral response curves, or computational optimizations.

3.5.1.1 Test Scenes

The VIIRS Surface Reflectance IP, surface reflectance (based on Lambertian Assumption) output files that have been generated are checked to ensure that the Lambertian surface reflectance was performed correctly. We obtained two test data cubes that best cover the range of conditions likely to be passed through the algorithm. The input files are VIIRS imagery-resolution and moderate-resolution SDRs generated from the MODIS L1b granule dated 2002, day 39, time 17:55 (herein termed the “Arizona” scene), and VIIRS imagery-resolution and moderate-resolution SDRs generated from the MODIS L1b granule dated 2002, day 150, time 14:05 (herein termed the “Amazon” scene). The corresponding MODIS L2 surface reflectance output files produced from the same MODIS granule used to produce the VIIRS SDRs will act as the ‘truth’ for this exercise.

Figure 10a shows the VIIRS sized granules over the Amazon rainforest in spring/summer, 2000 (‘dark target’, or “Amazon” scene), and Figure 10b shows the VIIRS sized granules over the desert and semi-arid areas of Mexico and the U. S. Southwest in early February, 2002 (‘bright target’, or “Arizona scene”).

(a)

A

(b)

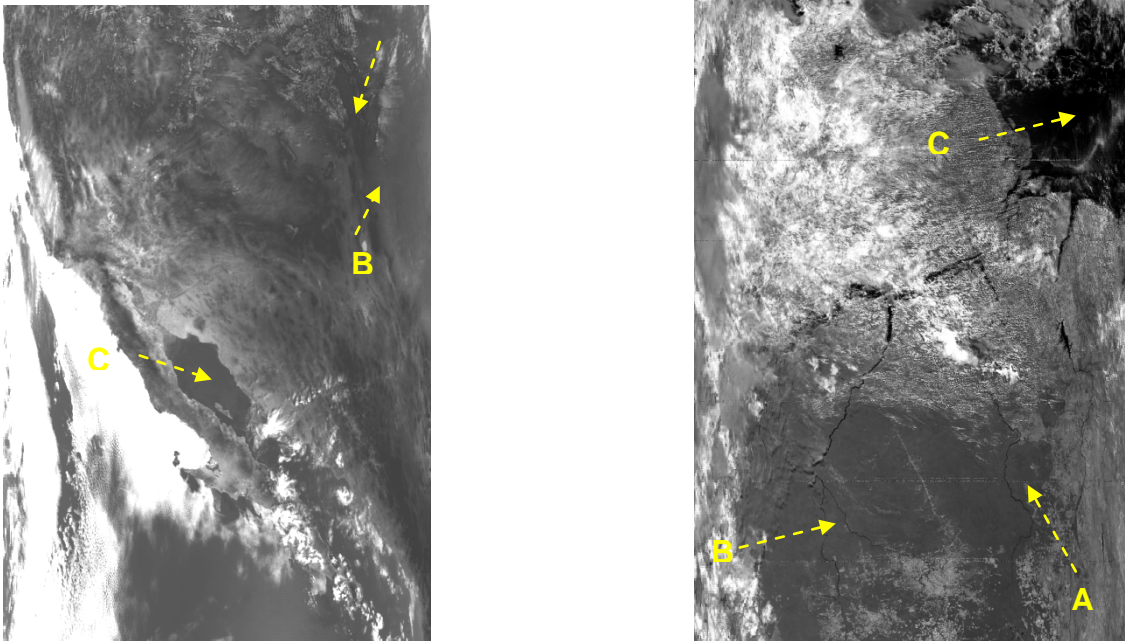


Figure 10. Test scenes centered over (a) the southwestern United States (i.e. 'bright' target area) and (b) the Amazon (i.e. 'dark' target area) used for the VIIRS Surface Reflectance algorithm validation.

The data cubes contain MODIS spectral data (e.g. spectral TOA reflectance values, geolocation, metadata, quality flags), and corresponding ancillary data, primarily geolocated atmospheric data were obtained for these 2 scenes. The MODIS data were run through a program that simply maps the MODIS data to the nearest VIIRS spectral band, and the nearest pixel. The ancillary data required to run the Surface Reflectance algorithm were regridded to a VIIRS format using a nearest neighbor-like method. Once these data were converted to VIIRS 'space', a VIIRS cloud mask was created for the scene by running the VIIRS Cloud Mask. These data were then input to the surface reflectance IP algorithm to create the output.

3.5.1.2 Results

Tables 3 & 4 highlight the expected comparison results between the VIIRS and the corresponding MODIS surface reflectance retrieval outputs assuming a Lambertian surface using Arizona and Amazon data cubes. The agreement between MODIS and VIIRS results may be better or worse depending on solar and viewing geometries, spatial differences, and spectral differences, for example. Generally, the greater these differences, the worse the agreement. Moderate resolution VIIRS output was chosen to minimize the spatial differences between VIIRS and MODIS. Similarly, comparing the outputs from VIIRS M4 and MODIS band 4 minimized spectral differences. Three points were selected to provide a test over water, a relatively dark land surface, and a relatively bright land surface. The VIIRS results from the processing algorithm at these points have also been compared to results directly from the 6S radiative transfer model to verify their validity.

The purpose of this test is to demonstrate that the compiled version of the delivered code can reproduce the results indicated in the Figures and Table in this section. The agreement between the MODIS and VIIRS bands seen here is within the expected range of results when comparing two systems with spatial and spectral differences, although, as described above, an attempt was made to minimize these differences when selecting the band used for this comparison. Table 3 highlights the comparison results between the VIIRS and the corresponding MODIS surface reflectance retrieval outputs assuming a Lambertian surface using the Arizona scene. The comparison is favorable as expected.

Table 3. Retrieved atmospherically corrected Surface Reflectance Values-Arizona Scene.

ID(see Figure 10A)	Latitude	Longitude	VIIRS Surf. Refl. M4	MODIS Surf Refl, band 4
A	38.9681	-101.8677	0.0973	0.1096
B	31.4797	-100.0861	0.066	0.0624
C	30.0545	-113.5852	0.0124	0.0085

Table 4 highlights the comparison results between the VIIRS and the corresponding MODIS surface reflectance retrieval outputs assuming a Lambertian surface using the Amazon scene. The comparison is favorable as expected.

Table 4. Retrieved atmospherically corrected Surface Reflectance Values-Amazon Scene.

ID(see Figure 10B)	Latitude	Longitude	VIIRS Surf. Refl. M4	MODIS Surf Refl, band 4
A	-6.4027	-50.82383	0.0263	0.0272
B	-8.7331	-56.86252	0.0382	0.0366
C	1.68867	-48.55374	0.0184	0.0129

3.5.1.3 Summary

The structure of the VIIRS Surface Reflectance IP algorithm was modified without significantly changing its scientific basis. The Surface Reflectance IP algorithm has a high potential of meeting its derived specifications despite the algorithm changes. That said, future calibration and validation efforts will be required to fine tune much of the areas not exhaustively investigated at this point, such as the aerosol properties and radiation coupling with water vapor, adjacency and BRDF adjustments, and the cirrus correction.

3.5.2 PREVIOUS SIMULATION TESTS

Previous sensitivity tests included:

- Phase I scene simulations using Terrain Categorization (TERCAT) scenes based on Landsat Thematic Mapper (TM) imagery
- Phase I “stick modeling” simulations that deal with the radiative transfer for a single linear path through the atmosphere
- Phase II stick modeling focused more exclusively on each individual error source, particularly those associated with the atmosphere.

In all three cases, MODTRAN was the primary forward model used. MODTRAN 3.7 (Kneizys *et al.*, 1996) was the basis for the Phase I efforts. MODTRAN 4.0 (Berk *et al.*, 1999) was used for Phase II simulations. See previous versions of this document for details. Additional simulations are planned.

3.6 ALGORITHM VALIDATION

Validation requires detailed knowledge of the relationship between processes and variables that may be used to monitor those processes over the full range of natural conditions. Pre-launch activities include determination of algorithms and characterization of uncertainties resulting from parameterizations and their algorithmic implementation. Post-launch activities include refinement of algorithms and uncertainty estimates based on near-direct comparisons with correlative data and selected, controlled analyses. The following provides a synopsis of the validation plan, which is detailed in VIIRS document Y3237.

3.6.1 Pre-Launch Algorithm Test/Development Activities

Pre-launch algorithm and system performance validation will be performed primarily with MODIS data, as the spectral bands are very similar and in many cases identical to those for VIIRS. The algorithm heritage is also quite similar for the two systems. The MODIS validation infrastructure, combined with international cooperative efforts such as Long Term Ecological Research (LTER) and the Global Terrestrial Observing System (GTOS), will allow for rigorous validation without high cost or risk. Existing data sets have already played a role and will continue to do so; an example would be the AVHRR and Thematic Mapper (TM) data collected in the Boreal Ecosystem/Atmosphere Study (BOREAS) to retrieve surface reflectances. The atmospheric inputs can be obtained from *in situ* measurements made during the field campaigns such as BOREAS. Aerosol optical thickness (AOT) can be obtained from sun photometer observations made by the Aerosol Robotic Network (AERONET); the atmospheric conditions may be obtained from other *in situ* measurements or climatological data sets. By comparing those retrieved surface reflectance values with other multi-angular airborne measurements (Polarization and Directionality of the Earth's Reflectances [POLDER], Advanced Solid-state Array Spectroradiometer [ASAS]), Portable Apparatus for Rapid Acquisition of Bidirectional Observations of Land and Atmosphere (PARABOLA) measurements, and albedo measurements, we will address the accuracy, uncertainty, and precision of the retrieved surface reflectance values at different cases, e.g., their dependencies on the angular sampling, surface conditions, and seasonal changes (for example, snow and no-snow background conditions).

3.6.2 Post-Launch Algorithm Test/Development Activities

Post-launch algorithm and system performance validation/verification will exist as a continuation of the activities formulated and applied pre-launch. Focus will be placed on leveraging existing infrastructures for validation, not just from MODIS activities, but on a global scale. The validation at the sensor level can be accomplished by performing what is known as a vicarious calibration. A vicarious calibration campaign is concerned with the sensor, and seeks to determine the most representative value of at-satellite-radiance. It should be conducted over a bright surface (such as sand, snow), a dark surface (such as a densely vegetated forest, water body), a moderately dark, homogeneous, vegetated body, and a moderately dark, non-homogeneous, vegetated body. A vicarious calibration should, at the least, be conducted over both bright and dark surfaces. The degree of homogeneity varies according to the particular sensor spatial & spectral properties as well as the solar & viewing geometries present during a particular overpass. The requirements for a vicarious calibration are:

- A complete dataset to predict top of the atmosphere radiance.
 - A complete dataset is defined as containing sensor characteristics, and ground truth and atmospheric data. For example, surface reflectance, other biophysical data as necessary, surface BRDF, and atmospheric data
 - Data should be obtained for a view as consistent with the satellite-borne sensor being calibrated.
 - Data should be collected for similar solar/target geometry.
- Known sensor characteristics.
 - What are the gains and biases of the satellite sensor being calibrated?
 - What are the sources of error to the gains and biases?
 - An estimate of how well the surface features from coarse resolution environmental satellites match the location and extent of surface features observed at high spatial resolution over the measurement period, and one month time period.
- Knowledge of how well the surface feature maps match the ground observations
 - Do surface reflectance instrumentation have solar geometry module(s) similar to that of the satellite sensor being calibrated?
 - What are the accuracy and precision characteristics of the ground-truthing instrumentation
 - How many data points were obtained to represent the feature space?
 - How well do the data reproduce the feature space? (or how well did the sampling optimization scheme work?)
- A determination of the likelihood that "ground truth" on surface feature maps can be extracted from satellite data (i.e., VIIRS, ETM+, MODIS) in the desired region.

The optimal measurement collection conditions for a vicarious calibration are high elevation, homogeneous sites, when the sun is highest in the sky and the atmosphere is as blue as it can be. Less optimal conditions include data collection on thin overcast days. Thin overcast is defined as being able to see the cloud's disk through the cloud or haze layer. The data

from these measurements could be useful, however. The data from these conditions since it could be instructive in comparison to optimal conditions. They will also provide a calibration and validation data to those developing cloud retrieval or QA/QC monitoring algorithms. Data collection should NOT occur on rainy days to prevent possible instrument damage from water and avoid the problems of impassable roads for example.

A likely instrumentation suite used in a vicarious calibration include a crop scan or preferably an ASD, sun photometer (or possibly shadow band radiometer), and GPS. An ASD is a hyper spectral version of the crop scan instrument. A ceptometer, fractional photosynthetic radiation (fPAR), and LAI-2000 sensors can be added if product validation activities are combined with calibration activities. The latter should be a common practice for a number of reasons, the most important of which is economics.

A standard procedure for the field measurement component of a Vicarious Calibration begins like any other field measurement campaign, namely getting the instruments ready for field use. The field campaign locations will be determined according to need and programmatic requirements and are not considered here. Recall that multiple sampling locations might need to be sampled simultaneously. It may also be possible that these multiple sampling areas reside in different scenes, in which case the following has to be modified and applied to each location. One should try to get all locations simultaneously during the overpass of the sensor. This is not always possible due to instrumentation, personnel and other resource limitations. Keep in mind that it takes approximately 40 minutes to cover a nine-pixel area within a Landsat 7 image using a cropsan using one person. A nine-pixel area (or approx. 100 m by 100 m) should be large enough to estimate BRDF and adjacency effects for this 9-pixel area's center. This may or may not encompass enough points to reproduce all features in the satellite sensor's corresponding pixel or scene, which is one reason for sampling at ancillary sites.

One might employ a tool that determines the optimum way to cover the primary and ancillary target areas given the available resources. Such a tool would combine spectral information from operational satellite imagery at preferably better resolution than VIIRS, to create a coefficient of spectral variance to identify regions of relative homogeneity at various biomass levels (i.e. as low, middle, or high NDVI).

Each chosen area should be sampled in a pattern that is similar to, and at a spatial frequency that is at least double that of the imagery grid spacing. The latter is important in satisfying the last requirement of the vicarious calibration. Suffice it to say that this could mean that the sampling campaign becomes very labor intensive depending on the horizontal resolution of the satellite sensor's image. The tool could be applied to intensify or relax this sampling requirement, which is simply set in order to ensure that the ground truth observations can be used to derive the 'true' field of the parameter (process) they were meant to measure. The calibration/validation plan [Y3237] should provide additional details, which should vary as a function of the product that is to be validated, and possibly as a function of the sensor that is calibrated.

The sampling crews should consist of at least 3 people; One to operate the cropsan or ASD; one to operate a ceptometer (or other instrument); the third to operate the Microtops II (or other sun photometer), take notes and, if trained, to mark (given permission) the measurement points (at least with a GPS unit). There should not be any more than 4 people to a sampling crew unless there is instrumentation in addition to what has already been mentioned. A reduced crew size could be accommodated if measurements are made in the vicinity of existing field measurement infrastructure, such as the Oklahoma Mesonet, DOE ARM Cart site, or the USGS EDC 'instrumentation farm' (DeFelice, 2000; Crane and DeFelice, 2003; DeFelice et al. 2004).

3.7 PRACTICAL CONSIDERATIONS

3.7.1 Numerical Computation Considerations

The Land module unit EDRs must be completely processed from VIIRS raw data, including calibration and geolocation, within 28 minutes from the time the raw data are available. This requirement is a strong reminder that VIIRS is an operational instrument with real-time user needs. For the Surface Reflectance IP, even though a pure LUT approach is no longer being employed, the challenges posed by the SRD timeliness requirement are not trivial. Application of a LUT with as many dimensions as listed in Version 5, revision 4 would require the use of advanced programming techniques to minimize search time and I/O. Even with the modified scheme, which uses several smaller LUTs rather than one large LUT to retrieve surface reflectance, the quantities of data involved and the complexities of the algorithm will make strong demands on operational processing resources. It will be vital to utilize state-of-the-art search and I/O methodologies along with parallel processing and other optimization methods to ensure the timeliness requirement is not endangered for this pivotal intermediate product. The VIIRS Surface Reflectance IP is required for a number of downstream products, so it will require completion far in advance of the 28-minute limit. Computation time for the weekly and monthly offshoots of Surface Reflectance is not expected to be an issue, as much of this burden can be moved offline. The computations involved are quite straightforward in any event.

3.7.2 Programming and Procedural Considerations

As noted in the previous section, one of the chief software challenges for Surface Reflectance is to maximize the efficiency of searching the LUTs. The necessity of aggregating data from the surrounding area in order to perform the adjacency correction to surface reflectance also imposes a burden on the timeliness of the VIIRS surface reflectance algorithm, making the adjacency routine an important candidate for optimization. It will also be important to ensure sufficient memory or storage to hold the VIIRS granule data, ancillary data, and LUTs at operational processing time. VIIRS Phase II efforts were largely software-focused, and the methodology for this development work was based on sound and proven principles, as discussed in the VIIRS Algorithm Software Development Plan [Y6635]. The present maturity of the VIIRS software is detailed in the VIIRS Algorithm Software Maturity Assessment document [Y6661]. The maturity and remaining Phase II tasks for the algorithms themselves is summarized in the VIIRS Algorithm/Data Processing Technical Report [Y7040]. The

software designs relevant to Surface Reflectance are summarized in the VIIRS Context Level Software Architecture [Y2469], Land Module Level Software Architecture [Y2474], Land Module Level Detailed Design [Y2483], and Surface Reflectance IP Unit Level Detailed Design [Y2498]. These designs will be tested at the system level as described in the most recent versions of the VIIRS Software Integration and Test Plan [Y3236], Algorithm Verification and Validation Plan [Y3237], and System Verification and Validation Plan [Y3270]. A summary of the ultimate strategy for operational application of the system of VIIRS algorithms is provided in the VIIRS Operations Concept document [Y2468]. The VIIRS Interface Control Document (ICD [Y2470]) provides more detail on the specifics of ancillary data requirements for Surface Reflectance and other VIIRS products.

3.7.3 Configuration of Retrievals

The primary adjustable parameters for the retrieval of the Surface Reflectance IP are those that govern the overall stratification with respect to the expected quality of the output. These parameters are summarized in Table 5. The values listed may evolve with time leading up to the launch of the VIIRS prototype, and again leading up to the launch of the first operational instrument.

Table 5. Configuration of parameters for Surface Reflectance retrievals.

Symbol	Description	Current Value
θ_{0ques}	Solar zenith angle at which retrievals are flagged as questionable	70°
θ_{0max}	Maximum allowable solar zenith angle	85°
f_{ques}	Threshold cloud fraction within pixel beyond which retrievals become flagged as questionable (probably clear, probably cloudy, and thin cirrus will be processed along with confident clear, but flagged)	0%
τ_{ques}	Threshold aerosol optical thickness beyond which retrievals become flagged as questionable	0.5
τ_{cques}	Threshold cirrus optical thickness beyond which retrievals become flagged as questionable	TBD
τ_{amax}	Maximum aerosol optical thickness beyond which retrievals will not be conducted	2.0
τ_{cmax}	Maximum cirrus optical thickness beyond which retrievals will not be conducted	TBD

A central task of Phase II was to develop and refine the Land Quality Flag (LQF) structure in detail. This data structure operationally indicates the quality of Surface Reflectance, Vegetation Index, Surface Albedo, Surface Type, Soil Moisture, and Active Fires. It is still in a dynamic state. The parameters listed in Table 5 formed a starting point for the LQF output structure.

3.7.4 Quality Assessment and Diagnostics

Operationally, quality control is automated for the Surface Reflectance IP, using the LQF output. The structure of these flags is detailed in the VIIRS Surface Reflectance Detailed Design Document [Y2483]. These flags and their structure will be refined, as the development effort gets closer to launch readiness. The final structure will likely contain a number of additional items more related to operational data transmission and processing.

3.7.5 Exception Handling

There are a number of situations encountered in practice that will preclude the accurate retrieval of the Surface Reflectance IP. In some instances, the degradation in accuracy is sufficiently small that the products are reported regardless. At other times, the degradation is high enough that retrieval becomes counterproductive. Table 6 summarizes the current sources of exceptions for Surface Reflectance product generations, along with a brief description of the strategy for dealing with each source. If any of these sources is present as a significant contributor to the degradation in the product, the user will be notified via a corresponding flag in the LQF output. A detailed description of the flags is given in the Operational Algorithm Description (OAD) document.

Table 6. Exception sources and handling strategies for Surface Reflectance retrievals.

Exception Source	Strategy
τ_a beyond τ_{aques}	Report, flag as obscured by aerosol
τ_a beyond τ_{amax}	Do not report, flag as missing
τ_c beyond τ_{acues}	Report, flag as obscured by cirrus
τ_c beyond τ_{cmax}	Do not report, flag as missing
Pixel flagged as confident cloudy, non-cirrus	Do not report, flag as missing
Pixel flagged as probably clear or probably cloudy, non-cirrus	Report, flag as possibly obscured by non-cirrus cloud
Solar zenith angle between θ_{0ques} and θ_{0max}	Report, flag as low illumination
Solar zenith angle higher than θ_{0max}	Do not report, flag as missing
Radiance(s) questionable	Report, flag as questionable

4.0 ASSUMPTIONS AND LIMITATIONS

4.1 ASSUMPTIONS

This ATBD has included the following assumptions:

1. The applicability and validity of 6S across the range of solar zenith and viewing zenith limits, cirrus and aerosol properties, and gaseous absorber amounts considered therein
2. The availability of necessary non-VIIRS input data for operational retrievals to the quality described in the VIIRS Interface Control Document [Y2470]
3. The availability of an aerosol climatology where aerosol retrievals cannot be performed directly over a large region
4. The feasibility of a software solution to safely fit the Surface Reflectance IP implementation into the VIIRS timeliness requirements

4.2 LIMITATIONS

Performance is not guaranteed under conditions of extreme aerosol loading, such as that associated with thick haze, biomass burning, local volcanic eruptions, or other similar events, which include but are not limited to the presence of optically thin clouds, including cirrus. The Surface Reflectance IP algorithm is state-of-the-science, especially with respect to its dynamic 'in-view' aerosol optical thickness input, adjacency adjustment, BRDF-coupling adjustment and thin cirrus correction. These state-of-the-science features are still considered research grade by our MODIS heritage scientists. Future calibration and validation efforts will be required to fine tune much of the areas not exhaustively investigated at this point, such as the aerosol properties and radiation coupling with water vapor, adjacency and BRDF adjustments, and the cirrus correction.

5.0 REFERENCES

Berk, A., G. P. Anderson, P. K. Acharya, J. H. Chetwynd, L. S. Bernstein, E. P. Shettle, M. W. Matthew, and S. M. Adler-Golden (1999). *MODTRAN4 User's Manual*. Air Force Research Laboratory, Space Vehicles Directorate, Hanscom AFB, MA 01731-3010.

Crane, M.P. and T.P. DeFelice, 2003. Enhancing the validation of remote Sensing data. AMS 12th SMOI, Long Beach, CA., 9-13 February, 001-001.

DeFelice, T.P., 2000. EDC Terrestrial-Ecosystem Assessment (TERESA) Site. Proc's USGS NMD Research Symposium, Apr. 25-27, Rolla, Missouri, 24-33.

DeFelice, T.P., and B.F. Wylie, 2001. Sky type discrimination using a ground based sunphotometer. *Atmos. Res.*, **59-60**, 313-329.

DeFelice, T.P., D. Lloyd, T.T. Baltzer, D.J. Meyer, P. Piraino, (2004). Water vapor correction of the daily 1-kilometer AVHRR global land dataset. Part I: Validation and use of the Water Vapor input field. *Int'l. J. Remote Sensing*, **24**(1), 001-011. In Press.

Deschamps P.Y., Herman M., Tanre D, 1983, Modeling of the atmospheric effects and its application to the remote sensing of Ocean Color, *Applied Optics* , 22 (23): 3751-3758.

Gao, B.-C., and Y.J. Kaufman (1993).. Water vapor retrieval from MODIS. In Vermote and Vermuelen (1998).

Hucks, J. (1998). VIIRS Testbed sensor modeling efforts, Phase I. Raytheon Systems Company Internal Memorandum Y1629.

IPO (2000). Visible/Infrared Imager/Radiometer Suite (VIIRS) Sensor Requirements Document (SRD) for National Polar-Orbiting Operational Environmental Satellite System (NPOESS) spacecraft and sensors, Rev. 3. Prepared by Assoc. Directorate for Acquisition, NPOESS Integrated Program Office, Silver Spring, MD.

Justice, C.O., E. Vermote, J.R.G. Townshend, R. DeFries, D.P. Roy, D.K. Hall, V.V. Salomonson, J.L. Privette, G. Riggs, A. Strahler, W. Lucht, R.B. Myneni, Y. Knjazikhin, S.W. Running, R.R. ~~Wan, A. R. Huete, W. van Leeuwen, R.E. Wolfe, L. Giglio, J.-P. Muller, P. Lewis, and M.J. Barnsley~~ (1998). The Moderate Resolution Imaging Spectroradiometer (MODIS): Land remote sensing for global change research, *IEEE Trans. Geosci. Remote Sens.*, 36, 1228-1249.

Key, J. R., P. Yang, B. A. Baum, S. L. Nasiri (2000). Parameterization of shortwave ice cloud optical properties for various particle habits. Submitted to *Journal of Geophysical Research*.
Kneizys, F.X., L.W. Abreu, G.P. Anderson, J.H. Chetwynd, E.P. Shettle, A. Berk, L.S. Bernstein, D.C. Robertson, P. Acharya, L.S. Rothman, J.E.A. Selby, W.O. Gallery, and S.A. Clough (1996). *The MODTRAN 2/3 Report and LOWTRAN 7 Model*. L.W. Abreu and G.P.

Anderson, eds. Prepared by Ontar Corporation, North Andover, Massachusetts, for Phillips Laboratory, Geophysics Directorate, Hanscom AFB, Massachusetts.

Lee, T. Y., and Y. J. Kaufman (1986). Non-Lambertian effects on remote sensing of surface reflectance and vegetation index. *IEEE Transactions on Geoscience and Remote Sensing*, GE-24, 699-708.

Liang, S., others (2002). Validating MODIS land surface reflectance and albedo products: methods and preliminary results. *Remote Sensing of Environment*, **83** 001-014.

Lyapustin, A.I. (2001). Three-Dimensional Effects in the Remote Sensing of Surface Albedo. *IEEE Trans Geosci Remote Sens.*, Vol 39, 001-009.

Running, S. W., C. Justice, V. Salomonson, D. Hall, J. Barker, Y. Kaufman, A. Strahler, A. Huete, J.-P. Muller, V. Vanderbilt, Z. M. Wan, P. Teillet and D. Carneggie (1994). Terrestrial remote sensing science and algorithms planned for EOS/MODIS. *Int. J. Rem. Sens.*, **15(17)**, 3587-3620

Tanré, D., B.N. Holben, and Y.J. Kaufman (1992). Atmospheric Correction algorithm for NOAA-AVHRR Products: Theory and Application. *IEEE Transaction on Geoscience and Remote Sensing*, **30**, 231-248.

Teillet, P.M. (1991). Radiometric and atmospheric correction procedures for AVHRR preprocessing in the solar reflective channels. *Proceedings of the Fifth International Colloquium on Measurements & Signatures in Remote Sensing, Courchevel, France*, Jan. 14-18, 101-104. Canada Centre Remote Sensing (CCRS) No. ESA-319; Remote Sensing on-line Retrieval System (RESORS) ID# 1083741. {Available from Author at CCRS, 588 Booth St., Ottawa, Ontario K1A 0Y7, Canada}.

Teillet, P.M. (1992). An algorithm for the radiometric and atmospheric correction of AVHRR data in the solar reflective channels. *Remote Sensing Environment*, **41**, 185-195.

Vermote, E.F. (2003). Adjacency effect. *Encyclopedia of Optical Engineering*, Marcel Dekker, Inc., NY, NY, 39-48.

Vermote, E.F., and A. Vermeulen (1999). Atmospheric correction algorithm: spectral reflectances (MOD09). Version 4.0. Algorithm technical background document. *NASA EOS-1D 2015 Doc*.

Vermote, E.F., D. Tanré, J.L. Deuzé, M. Herman, and J.J. Morrisette (1994). Second Simulation of the Satellite Signal in the Solar Spectrum (6S), 6S Version 0 User's Guide, April 18. *NASA Goddard Space Flight Center*, 183 pp.

Vermote, E.F., D. Tanré, J.L. Deuzé, M. Herman, and J.J. Morrisette (1997). Second Simulation of the Satellite Signal in the Solar Spectrum, 6S: An Overview. *IEEE Transactions on Geoscience and Remote Sensing*, **35**, 675-686.

Vogelmann, J.E., and T.P. DeFelice (2003). Characterization of intra-annual reflectance properties of land cover classes in southeastern South Dakota using Landsat TM and ETM+ data. *Can. J. Remote Sens.* **29**(2), 219-229.